

Nemotron-H: A Family of Accurate and Efficient Hybrid Mamba-Transformer Models

NVIDIA

Abstract. As inference-time scaling becomes critical for enhanced reasoning capabilities, it is increasingly becoming important to build models that are efficient to infer. We introduce Nemotron-H, a family of 8B and 56B/47B hybrid Mamba-Transformer models designed to reduce inference cost for a given accuracy level. To achieve this goal, we replace the majority of self-attention layers in the common Transformer model architecture with Mamba layers that perform constant computation and require constant memory per generated token. We show that Nemotron-H models offer either better or on-par accuracy compared to other similarly-sized state-of-the-art open-sourced Transformer models (e.g., Qwen-2.5-7B/72B and Llama-3.1-8B/70B), while being up to $3\times$ faster at inference. To further increase inference speed and reduce the memory required at inference time, we created Nemotron-H-47B-Base from the 56B model using a new compression via pruning and distillation technique called MiniPuzzle. Nemotron-H-47B-Base achieves similar accuracy to the 56B model, but is 20% faster to infer. In addition, we introduce an FP8-based training recipe and show that it can achieve on par results with BF16-based training. This recipe is used to train the 56B model. All Nemotron-H models will be released, with support in Hugging Face, NeMo, and Megatron-LM.

1. Introduction

Attention (Vaswani et al., 2023) traditionally has been the powerhouse of large language models (LLMs). Yet, to generate one token during auto-regressive inference, the self-attention layer must perform computation that scales linearly with the number of tokens seen so far since it models interactions between all pairs of tokens in a sequence (potentially in a causal way); as a result, self-attention layers also have to store state in a KV cache during inference that is linearly proportional to the number of tokens in the sequence (Kwon et al., 2023). Recent reasoning LLMs, however, exhibit *inference-time scaling*, where generating more tokens at inference time can improve the quality of model responses (OpenAI, 2025; DeepSeek-AI, 2025a). Thus, attention layers can fundamentally limit overall model intelligence.

To address this issue, much recent work has proposed alternative architectures (Katharopoulos et al., 2020; Beltagy et al., 2020; Gu & Dao, 2024; Dao & Gu, 2024). One such example is a series of *hybrid models* that replace the majority of the self-attention layers in the standard Transformer architecture with more efficient layers (e.g., Mamba, Mamba-2, or sliding-window attention layers) that have sub-linear or even constant compute and memory requirements. Recent work has shown hybrid models to be competitive with more traditional Transformer architectures (Waleffe et al., 2024; Lieber et al., 2024; DeepMind, 2025).

Motivated by improving inference efficiency, we introduce the Nemotron-H family of hybrid Mamba-Transformer models. The Nemotron-H models consist of a mixture of Mamba-2, self-attention and MLP layers, and achieve state-of-the-art accuracy and improved inference speed when compared to open-sourced Transformer models of similar size (Figure 1). The Nemotron-H family has a series of 8-billion-parameter models (Nemotron-H-8B-Base, Nemotron-H-8B-Instruct, Nemotron-H-8B-VLM), and a series of 47/56-billion-parameter models (Nemotron-H-47B-Base, Nemotron-H-56B-Base, Nemotron-H-56B-VLM) that offer either better or on-par accuracy compared to

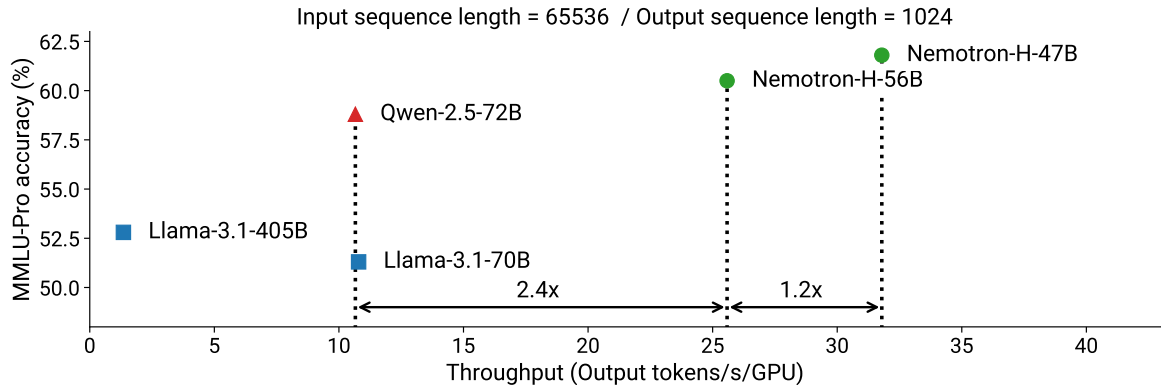


Figure 1 | MMLU-Pro accuracy (Wang et al., 2024) versus per-GPU inference throughput for Nemotron-H-56B/47B-Base compared to existing similarly-sized Transformer models. Nemotron-H models provide state-of-the-art accuracy and inference time speedups.

Qwen-2.5-7B/Llama-3.1-8B and Qwen-2.5-72B/Llama-3.1-70B, respectively. For example, Nemotron-H-56B-Base outperforms Llama-3.1-70B on 16 out of 17 tasks that we evaluated (§2.5). With larger sequences (65536 input sequence length, 1024 output tokens), we measure up to $3\times$ higher inference throughput on NVIDIA H100 GPUs.

To achieve the above results, we pre-train Nemotron-H models on up to 20 trillion tokens of high-quality curated and synthetically-generated data (Su et al., 2024; Akter et al., 2024). Nemotron-H-56B-Base is the first Nemotron model to be fully pre-trained using a FP8-based recipe. Our recipe, called per-tensor current scaling, is coarse grained and involves quantizing entire tensors using a single scaling factor. This factor is chosen to preserve the largest value in the given tensor; any value too small to fit in the desired FP8 format is flushed to zero. In addition, we find it important for training stability and convergence to leave the first and last 4 GEMMs of the model in BF16. In smaller ablations with 8B-parameter models on token horizons up to 15 trillion tokens, we show that FP8 per-tensor scaling can reach equal or better downstream task accuracy compared to BF16.

To efficiently tailor Nemotron-H models for different deployment scenarios, we introduce a new compression via pruning and distillation paradigm, called MiniPuzzle, that combines the simplicity of Minitron (Sreenivas et al., 2024) and the versatility of Puzzle (Bercovich et al., 2024). MiniPuzzle can be used to turn a larger model into a smaller model satisfying specific memory, parameter count, or latency constraints. We use MiniPuzzle to distill Nemotron-H-56B-Base to Nemotron-H-47B-Base, using only 63 billion training tokens and FP8 training. Nemotron-H-47B-Base can be deployed in FP4 precision on a single NVIDIA RTX 5090 GPU with 32GiB of memory (Nemotron-H-56B-Base’s model weights would require roughly 29.5GiB alone, limiting maximum context size).

The Nemotron-H base models can also be effectively post-trained to produce models with high accuracies on vision-language, instruction following, and long-context (e.g., RULER) benchmarks. Vision-Language Models (VLMs) based on both Nemotron-H-8B and Nemotron-H-56B have already been used to develop very strong reasoning models for physical AI as part of the Cosmos-Reason1 project (NVIDIA et al., 2025).

Overall, the Nemotron-H family of models demonstrates that hybrid models can be state-of-the-art in terms of capabilities while offering improved inference speed. Moreover, we believe FP8 pre-training and compression techniques like MiniPuzzle can make it cheaper and more efficient to create such models. To enable further research, we are releasing the models discussed in this report.

The rest of this technical report is organized as follows:

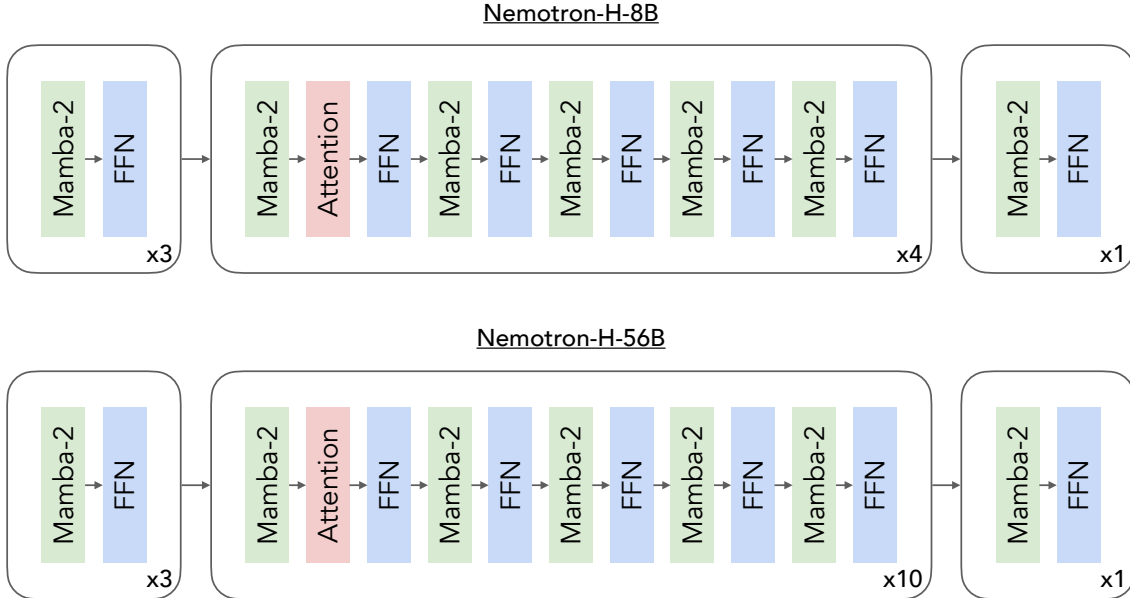


Figure 2 | Nemotron-H-8B/56B model architectures. Roughly 8% of the total layers in the model are self-attention layers; these layers are evenly dispersed throughout the model. The rest of the model is made up of alternating Mamba-2 and FFN layers.

- In §2, we discuss the Nemotron-H model architecture and the pre-training process (including details on the pre-training dataset and FP8 recipe used).
- In §3, we describe the pruning and distillation methods used for model compression.
- In §4, we introduce the vision-language models based on the Nemotron-H models.
- In §5, we show that Nemotron-H models can be extended to create competitive instruct and long-context versions.

2. Base Models and Pre-Training

In this section, we discuss the Nemotron-H-8B-Base and Nemotron-H-56B-Base model architectures, as well as key details in the pre-training process used to produce these models. We also compare Nemotron-H-8B/56B-Base with existing open-source state-of-the-art Transformer models on both accuracy (on common benchmark tasks used for base models) and inference speed.

2.1. Model Architecture

Nemotron-H models consist of a mixture of Mamba-2 (Dao & Gu, 2024), self-attention, and FFN layers as summarized in Figure 2 and Table 1. As suggested by prior work (Waleffe et al., 2024), we set the number of attention layers to be roughly 8% of the total number of layers and evenly disperse them throughout the model. This amounts to 4 self-attention layers (out of 52 layers) for Nemotron-H-8B and 10 for Nemotron-H-56B (out of 118 layers). The rest of the layers consist of an even split between FFN and Mamba-2 layers. We also ensure that a) the first layer in the model is a Mamba-2 layer, b) the last layer in the model is a FFN layer, and c) self-attention layers always precede FFN layers (as they do in a standard Transformer block like in Vaswani et al. (2023)).

We use a hidden dimension of 4096 for Nemotron-H-8B and 8192 for Nemotron-H-56B. For our smaller model, we use FFN hidden dimension of 21504, 32 attention query heads, and Mamba-2 state dimension of 128; for the larger model, we use FFN hidden dimension of 32768, 64 attention query

Model	Number of layers	Model dimension	FFN dimension	Q heads	KV heads	State dimension	Mamba groups
Nemotron-H-8B	52	4096	21504	32	8	128	8
Nemotron-H-56B	118	8192	32768	64	8	256	8

Table 1 | Summary of the Nemotron-H hybrid Mamba-Transformer architectures.

heads, and Mamba-2 state dimension of 256. Both models use Grouped-Query Attention (Ainslie et al., 2023) with 8 key-value heads, 8 Mamba-2 groups, and squared ReLU (So et al., 2022) activation for FFN layers. We do not use any position embeddings. For Mamba-2 layers, we retain the default values for head dimension (64), expansion factor (2), and window size for convolution (4). We also use RMSNorm (Zhang & Sennrich, 2019) for normalization, separate embedding and output layer weights, and no dropout. We do not use bias weights for linear layers. We include a residual skip connection around each Mamba-2, self-attention, and FFN layer in the architecture.

Nemotron-T-8B Transformer baseline. To compare Nemotron-H-8B-Base to a Transformer model in an apples-to-apples fashion, we also trained Nemotron-T-8B-Base on exactly the same data. The Nemotron-T-8B architecture follows the style of GPT-3 (Brown et al., 2020). We use 32 Transformer layers (each has a self-attention layer followed by a FFN layer). As for Nemotron-H-8B, we use a hidden dimension of 4096, 32 query heads, GQA with 8 key-value heads, a FFN hidden dimension of 21504, squared ReLU activation, RMSNorm, no bias weights for linear layers, no dropout, and separate parameters for model embeddings and output layer weights. We use RoPE for position embeddings (Su et al., 2023).

2.2. Pre-Training Data

Nemotron-H-8B-Base and Nemotron-H-56B-Base are pre-trained on a large corpus of high-quality curated and synthetically-generated data.

2.2.1. Curated Data

We have separate data curation pipelines for four broad data categories: general web crawl data, math data, code data, and “academic” data. We discuss each in turn next.

Web crawl data. For Nemotron-H, we made several key innovations in our processing of English Common Crawl data compared to Nemotron-4 (Parmar et al., 2024; NVIDIA, 2024); these innovations substantially improved data quality. For full details on how this dataset was prepared and various ablations, please refer to the dedicated paper (Su et al., 2024). We provide a brief summary here.

We focus primarily on extracting as many high quality tokens as possible, so that we can train Nemotron-H for long token horizons (e.g., 15 trillion or more tokens). As is common, we begin with HTML-to-text extraction, language filtering, global fuzzy de-duplication, and exact substring de-duplication. At this stage, however, we deviate from the norm and employ an ensemble of three model-based classifiers to bucket each document into five quality categories. By using an ensemble, we obtain a larger and more diverse set of high-quality tokens compared to approaches that use a single model-based classifier. To retain as many high-quality tokens as possible, we apply heuristic and perplexity filters to the low, medium-low, and medium quality buckets. We also rephrase the low-quality tokens to boost their quality; §2.2.2 describes the synthetic data generation pipeline.

The resulting dataset consists of 6.3 trillion tokens, including 4.4 trillion globally de-duplicated

Quality label	Tokens (billions)	Tokens (%)
High	554	8.8
Medium-High	505	8.1
Medium	2026	32.4
Medium-Low	896	14.3
Low	403	6.4
Synthetic-High	1536	24.6
Synthetic-Low	336	5.4

Table 2 | Quality distribution of the 6.3 trillion English Common Crawl tokens.

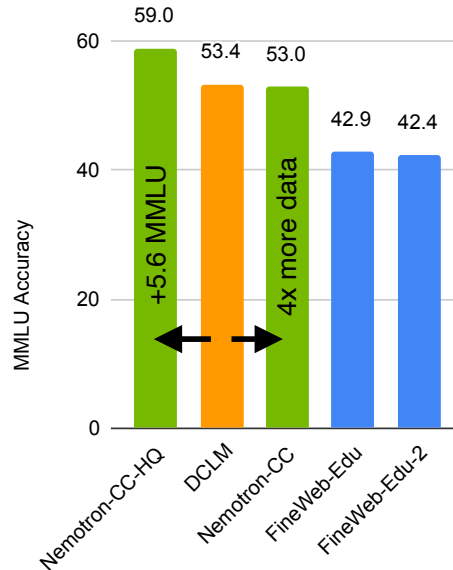


Figure 3 | MMLU scores for 8B-parameter models trained for 1 trillion tokens. Compared to DCLM, our methods enable us to either create a 4× larger dataset of similar quality or increase the MMLU using a high quality subset of the tokens. Having a larger dataset (in terms of unique tokens), is crucial when training over long horizons (e.g., 15 or 20 trillion tokens).

“real” tokens and 1.9 trillion tokens of rephrased synthetic data. The quality distribution is shown in Table 2. As shown in Figure 3, our dataset results in higher-quality models compared to other leading English Common Crawl preparations like DCLM (Li et al., 2024) and FineWeb-Edu (Penedo et al., 2024): using a high-quality subset increases MMLU by 5.6 points over DCLM, whereas using the full dataset without any weighting of quality buckets achieves comparable accuracy to DCLM while having 4× more unique tokens. Having more unique tokens enables pre-training over longer token horizons without having to do more than 4 to 8 epochs over the full dataset. Higher epoch counts lead to diminishing returns (Muennighoff et al., 2024; Feng et al., 2024).

For the benefit of the community, we have publicly released the dataset (as Nemotron-CC¹) under the Common Crawl terms of use.

Math data. To ensure that technical pages in Common Crawl retain their mathematical content, we leverage the recipe and code base from Paster et al. (2023). We also find it essential to apply this recipe to other high-quality data sources such as Wikipedia. We found that a smaller, higher-quality dataset led to a larger improvement on relevant benchmarks, similar to FineMath (Allal et al., 2025).

¹<https://data.commoncrawl.org/contrib/Nemotron/Nemotron-CC/index.html>.

Source	Raw tokens	Prompt	Synthetic tokens
Low	403.0	Wikipedia	336.3
		Wikipedia	372.9
High	451.3	Diverse QA Pairs	499.5
		Distill	157.6
		Extract Knowledge	303.6
		Knowledge List	203.2

Table 3 | Synthetic data token counts (billions) for web crawl, generated with the instruct version of Mistral NeMo 12B.

Code data. We pre-train Nemotron-H models with a considerable number of code tokens. We started from our previous work on Nemotron-4 (Parmar et al., 2024; NVIDIA, 2024), and chose to reduce the number of tokens in markup and configuration languages such as HTML, Markdown, YAML, CSS, JSON, and Makefile. Tokens that would have previously come from these languages are instead taken from popular languages like Python, C++, C, and Java.

Academic data. The Nemotron-H pre-training dataset contains additional tokens gathered from “high information” English texts, including permissively-licensed books and articles. We utilize examples across a wide variety of domains (e.g., science, math, humanities, law, and engineering) and a large range of document types including peer-reviewed journal publications, textbooks, published novels, and patent documents.

As the original data formats of these documents range widely—including EPuB, HTML, XML, plain text, PDF, LaTeX, and markdown—we write custom functions to parse text from the input format into a standardized output format. We maintain appropriate formatting in markdown or LaTeX for complex segments like tables, lists, and equations. We utilize Éclair (Karmanov et al., 2025) for PDF-to-text extraction. We also develop specialized heuristic filters to remove extraneous information contained within headers or footers of pages. We then apply the Nemotron-4 heuristic and perplexity filters to remove low-quality documents from the set of documents used for pre-training.

In order to better weight examples from these sources in our final data blend, we developed classifiers to rate documents on their educational content and difficulty. We also try to determine each document’s domain (one of biology, business, chemistry, computer science, economics, engineering, history, law, mathematics, medicine, philosophy, physics, psychology, or other). For educational content, we rated all documents on a numerical scale from 0 (no educational information) to 3 (highly relevant educational information). For educational difficulty, we categorized documents with high educational content into the following levels: elementary school, middle school, high school, undergraduate, and graduate. We were able to use these buckets (e.g., “biology at the undergraduate level with high educational content”) to determine document weights (§2.2.3). As expected, we found increasing the weight of highly educational content in important domains at the high school / undergraduate levels to be most helpful.

2.2.2. Synthetically-Generated Data

We also synthetically generate data to de-noise low-quality data and to increase the diversity of tokens given to the model. We use different processing pipelines to synthetically re-write web crawl, math, and code data.

Web crawl data. We found rephrasing text by LLMs to be an effective way to reduce noise and errors in low-quality crawl data, and produce additional variants of high-quality data with new unique tokens. This leads to better results on downstream tasks.

We rephrased our low-quality data using the “medium Wikipedia” prompt from [Maini et al. \(2024\)](#). For high-quality documents, we generated synthetic data using four additional prompts:

1. **Diverse question-answer (QA) pairs.** Ask questions in various forms (e.g., yes/no question, open-ended question, multi-choice question) about factual information in the text.
2. **Distill.** Rewrite the text into a concise and clear passage.
3. **Extract knowledge.** Rewrite knowledge from the text and disregard uninformative content.
4. **Knowledge list.** Extract key information from the text as an organized list.

These prompts required the model to provide clear and concise responses while preserving factual information and concrete details such as numbers. In total, we generated over 1.8 trillion synthetic tokens using the instruct version of Mistral NeMo 12B. The breakdown of source and generated tokens by quality and prompt is shown in Table 3. The full details of this synthetic data generation, including the prompts used, have been published separately in [Su et al. \(2024\)](#).

Math data. We use synthetic data to enhance mathematical reasoning benchmarks like GSM8K and MATH ([Cobbe et al., 2021](#); [Hendrycks et al., 2021b](#)), as detailed in [Akteer et al. \(2024\)](#). We expand OpenWebMath ([Paster et al., 2023](#)) from 14 billion to over 100 billion tokens using Nemotron-4-340B ([NVIDIA, 2024](#)), yielding an 18-point improvement on GSM8K in controlled experiments.

To achieve this, we start with technical pre-training documents from Common Crawl and leverage Nemotron-4-340B to generate dialogues, where a knowledgeable persona guides a less-experienced one (e.g., an interaction between student and teacher). This approach aligns with insights from the Physics of Language Models series ([Allen-Zhu & Li, 2024](#)), and incorporates strategies such as presenting incorrect answers alongside corrections. By structuring content as learning interactions, our method distills broad knowledge from public language models without overfitting to benchmarks.

Code data. With the goal of adding diverse code data centered around problem solving, we chose to synthetically generate mixed natural language and code datasets across 11 programming languages, e.g., Python, C++, C, C#, and Java. To do this, we prompted Mixtral 8x22B to generate a programming problem inspired by sampled pieces of source code from our curated code dataset. The samples range from 1 to 15 lines of code (LOC), and typically are just a small function. We also prompted Mixtral 8x22B to solve the generated problems and removed clearly invalid solutions on a minimal-effort basis. For example, we extracted the Python code generated by the model and attempted to parse it into an abstract syntax tree (AST), discarding samples which fail to parse. Finally, to form a sample for training, we combined the generated problem and answer into a single sample which is a mix of natural language instruction, generated code (typically enclosed in a markdown code block), and usually an explanation of the approach.

SFT-style data. We further add synthetic SFT-style data to the pre-training corpus; this improves the ability of base models to follow instructions. We use the Qwen2.5 series, Mixtral 8x22B, Nemotron-4-340B, and DeepSeek-R1 (only for 56B) models to produce these datasets. We improve math abilities following the pipeline presented in OpenMathInstruct-2 ([Toshniwal et al., 2024](#)) using carefully curated seed data such as AoPS². We also synthesize code data using the approach proposed in Genetic Instruct ([Majumdar et al., 2024](#)), with `tigerbot-leetcode`³ and

²<https://artofproblemsolving.com>.

³<https://huggingface.co/datasets/TigerResearch/tigerbot-kaggle-leetcodesolutions-en-2k>.

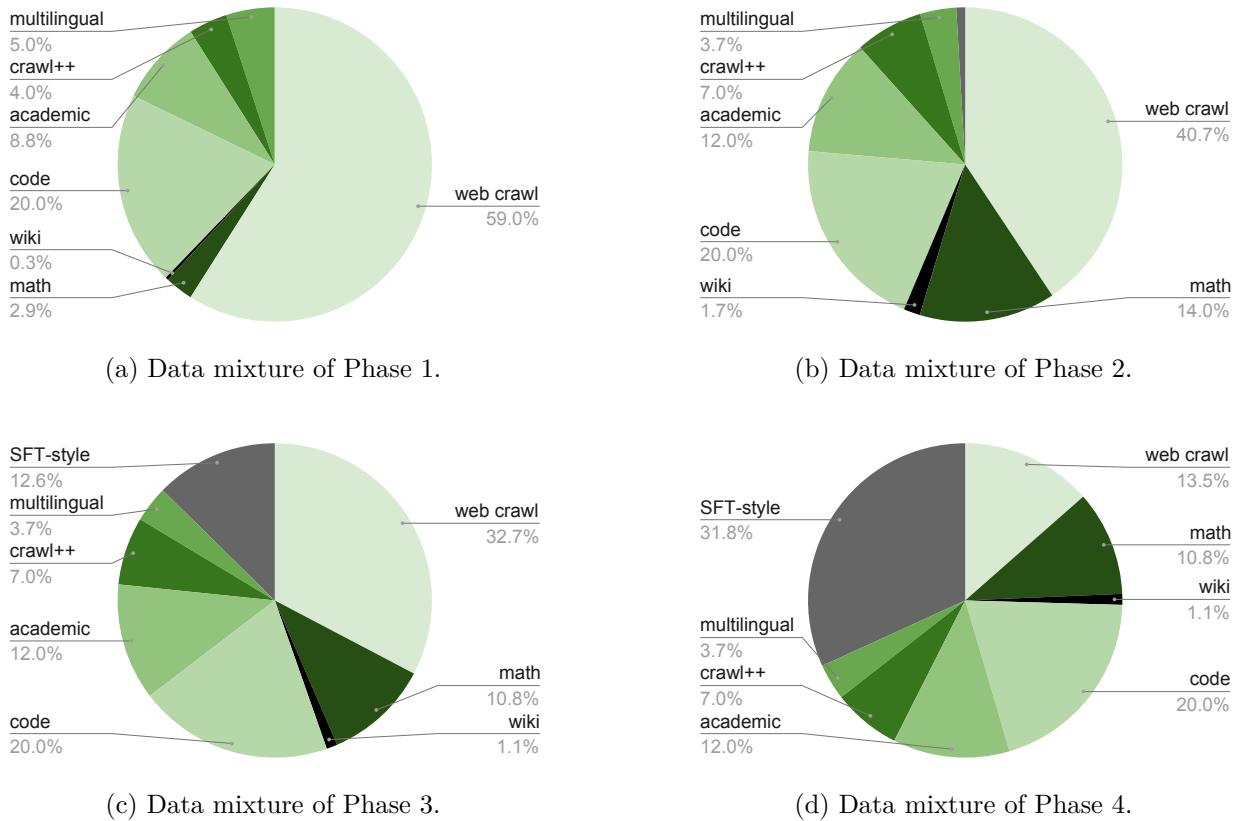


Figure 4 | Data mixtures for each phase of Nemotron-H pre-training.

`the-stack-v2`⁴ as seed data. In order to equip the base model with high-quality general knowledge, we generate question-solution pairs with selected topics and domain-specific documents. In total, we add 230 billion synthetic SFT-style tokens (174 billion math tokens, 35 billion code tokens, and 21 billion tokens with general knowledge) to the training corpus.

2.2.3. Data Mixture and Ordering

Our data mixture consists of seven high-level data categories: web crawl, math, wikipedia, code, academic, crawl++, multilingual, and synthetic SFT-style data. Crawl++ consists of web-crawl derivatives like OpenWebText, BigScience and Reddit. Our multilingual data has nine languages: German, Spanish, French, Italian, Portuguese, Chinese, Japanese, Korean, and Russian. We design the data mixtures in such a way that all data sources of a given quality are weighed similarly, and data sources of higher quality are weighed higher than data sources of lower quality. We provide more details on estimating the quality of datasets in Feng et al. (2024).

We use a phased data-blending approach (Feng et al., 2024) to pre-train both Nemotron-H base models. In the first phase, we use a data mixture that promotes diversity in data; in the second and third phases, we primarily use high-quality datasets (e.g., Wikipedia). We switch to the second phase at the 60% point of training, and to the third phase at the 80% point of training. The fourth phase is performed for the last 380 billion training tokens. The data mixtures used in each phase are shown in Figure 4. Our initial experiments on a 8-billion-parameter model trained on 1 trillion tokens show that a phased approach for pre-training outperforms random data ordering by 3.4%.

⁴<https://huggingface.co/datasets/bigcode/the-stack-v2>.

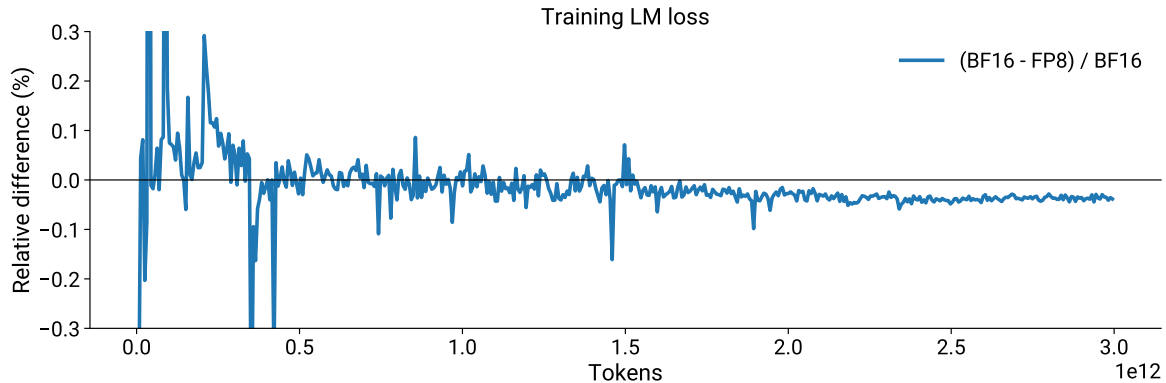


Figure 5 | The relative training loss gap between a pair of 8B-parameter Transformer models trained for 3 trillion tokens in BF16 and FP8. The gap is initially large, then shrinks, and then grows again in the last stage of training.

2.3. FP8 Recipe

Nemotron-H-56B-Base was pre-trained using layer-wise mixed precision: all linear layers in the model (including both linear layers in FFN blocks and the QKV / output projection in the attention block) were computed in FP8 precision, except the first 4 and last 4 layers, which were kept in BF16. We quantized both the forward and backward passes of the linear layers. As in [Micikevicius et al. \(2022\)](#), we use a hybrid FP8 approach which uses E4M3 for weight and activation tensors, and E5M2 for the gradient tensors.

We used FP8 per-tensor dynamic quantization, which has several steps: we first compute a quantization scale (with a check for division by zero); then, we multiply the input tensor with the quantization scale and cast it to the desired FP8 format. The quantization scale is computed as a ratio of the maximum representable value for that FP8 data format divided by the maximum absolute value of the input tensor. There are several options of floating-point rounding ([NVIDIA, 2025](#)) which can be used during the quantization scale computation. We noticed that downstream tasks were sensitive to this choice and rounding towards zero led to the best results.

We observed that the log-likelihood loss curves for FP8 pre-training experiments were almost always higher than for their BF16 counterparts, but by a surprisingly small amount, with typical relative gaps less than 0.1% on both training and validation. This loss gap tended to decrease as training progressed but then widened in the last quarter of training. We conjecture that this is because extremely small gradient updates, which dominate the latter parts of training, get flushed to zero despite operating in E5M2. Figure 5 shows a typical relative loss gap between a BF16 and FP8 experiment during pre-training.

Despite the marginally worse loss curves, we observed that downstream evaluations for models trained with FP8 were as good or better than BF16 experiments. Log likelihood, which has traditionally served as a proxy for downstream task, was not a reliable predictor in our experiments; in fact, we often observed models with better loss curves to perform worse on downstream evaluation tasks.

For coding and math tasks, experiments using per-tensor current scaling often had results that were substantially better than BF16 experiments. Figure 6 shows the accuracy gap between two 8B-parameter Transformers trained for 15 trillion tokens, with one trained in FP8 and the other in BF16. Because of the equal or better downstream results on the same token horizon, we never had to overtrain FP8 models relative to BF16 ones. We ran evaluations in both BF16 and FP8 precision for models trained in FP8; they were typically the same, with BF16 evaluations usually slightly

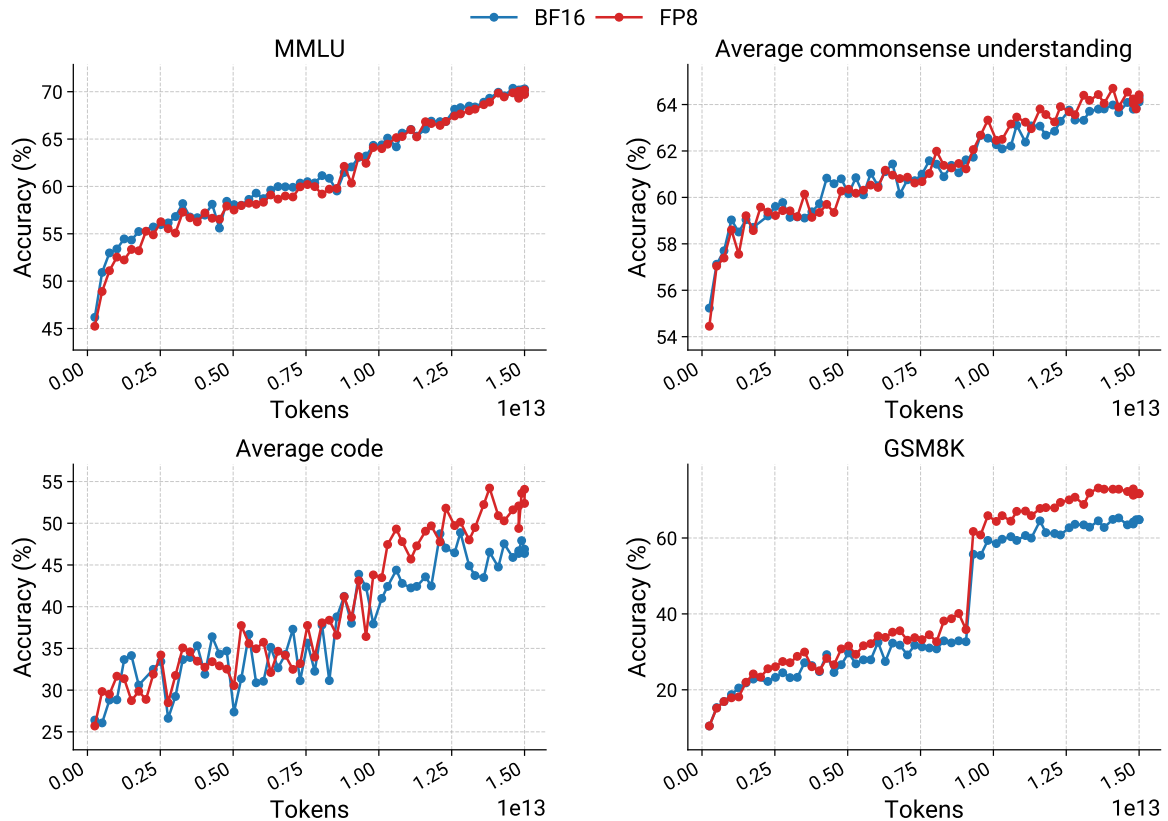


Figure 6 | Downstream task accuracies for a pair of 8B-parameter Transformer models trained on 15 trillion tokens with BF16 and mixed precision FP8. FP8 accuracies are consistently equal to or better than BF16 ones. The jump in accuracies at 9 trillion tokens is a result of switching data mixtures from Phase 1 to Phase 2.

better. However, for the 56B model, the FP8 evaluations eventually outperformed the BF16 ones.

We found it very important to do verification on a minimum of 8B parameters when constructing our FP8 recipe, as results with smaller models did not generalize. All experiments used token horizons of at least 1 trillion tokens.

2.4. Pre-Training

We trained Nemotron-H-8B-Base on a token horizon of 15 trillion tokens and Nemotron-H-56B-Base on a token horizon of 20 trillion tokens. We used a sequence length of 8192 and global batch size of 768 (6291456 tokens per batch). We do not use any batch size ramp-up. For Nemotron-H-8B-Base, we used a peak learning rate of $8 \cdot 10^{-4}$ and warmup over 8.3 billion tokens; for Nemotron-H-56B-Base, we used a peak learning rate of $4 \cdot 10^{-4}$ and warmup over 25 billion tokens. In both cases, we used cosine learning rate decay with a minimum value equal to 1% of the peak value, weight decay of 0.1, and 0.9 and 0.95 for Adam β_1 and β_2 , respectively

We pre-train Nemotron-H using Megatron-LM⁵; we rely on Transformer Engine⁶ for FP8 support. We use 8-way tensor model parallelism (Shoeybi et al., 2020) with sequence parallelism (Korthikanti et al., 2022) for additional memory savings, and 768-way data parallelism with optimizer state

⁵<https://github.com/nvidia/megatron-lm>.

⁶<https://github.com/nvidia/transformerEngine>.

distributed over the data-parallel replicas (Rajbhandari et al., 2020).

2.4.1. Resiliency

We also focus heavily on minimizing downtime when training models at scale: over long training jobs on a large number of GPUs, job failures and slowdowns are inevitable, leading to lost training productivity. Failures can occur due to GPU-related errors (e.g., uncorrectable ECC errors or GPUs falling off the bus), errors in shared infrastructure like the network fabric or Lustre, or application-induced failures (e.g., numerical instability in certain operations or “bad” data). We can also experience job slowdowns due to a variety of reasons (e.g., single-GPU throttling or slower communication collectives).

To minimize the impact of the above issues, we focus on a) accurately attributing failures to the correct infrastructure and application components to prevent repeated disruptions, and b) reducing the recovery overhead of each failure. To do so, we leverage the DGX Cloud Resilience service⁷ to ensure failures are correctly attributed and the appropriate hardware component (e.g., particular HGX node with failing GPU) is not included in the next instance of the training job, preventing repeated failures. With DGX Cloud Resilience enabled, we obtained a 3.3× improvement in mean time between failures (MTBF) in our cluster.

We also proactively save checkpoints frequently in order to minimize the amount of work lost when a failure occurs (weight updates from the last checkpoint save to the failure are lost). We use NVRx⁸ to facilitate checkpointing with low overhead by asynchronously saving checkpoints without blocking training. We also optimized job restart times (i.e., the set of operations needed by Megatron-LM before training iterations can start like distributed runtime initialization and checkpoint loading).

Altogether, the above components enable us to train Nemotron-H-56B-Base with high efficiency on 6144 NVIDIA H100 GPUs.

2.5. Base Model Evaluations

We run evaluations of all models ourselves unless otherwise stated. Our evaluation setup is built on top of `lm-evaluation-harness`⁹ for fair comparisons, with the following changes:

1. For mathematical reasoning, we evaluate on the GSM8K and MATH (Cobbe et al., 2021; Hendrycks et al., 2021b) benchmarks. We also highlight the competition-level slice of the MATH benchmark as “MATH Level 5”. After carefully looking through disagreeing cases, we use a combination of `Math-Verify`¹⁰ and the math grading utilities of `NeMo-Skills`¹¹ to grade solutions.
2. We also include a MATH-R1 version of the MATH task, where we provide few-shot examples generated by DeepSeek-R1 (DeepSeek-AI, 2025a). Both Nemotron-H and the Qwen 2.5 models show significant improvement on the benchmark by simply changing the prompt.
3. For code tasks (HumanEval (Chen et al., 2021), MBPP (Austin et al., 2021) and their EvalPlus variants), we always sanitize the generations using EvalPlus (Liu et al., 2023b).
4. General reasoning benchmarks (OpenBookQA (Mihaylov et al., 2018), PIQA (Bisk et al., 2019), Hellaswag (Zellers et al., 2019), Winogrande (Sakaguchi et al., 2019)) are unchanged

⁷<https://developer.nvidia.com/blog/ensuring-reliable-model-training-on-nvidia-dgx-cloud/>.

⁸<https://github.com/NVIDIA/nvidia-resiliency-ext>.

⁹<https://github.com/EleutherAI/lm-evaluation-harness>.

¹⁰<https://github.com/huggingface/math-verify>.

¹¹https://github.com/NVIDIA/NeMo-Skills/blob/main/nemo_skills/code_execution/math_grader.py.

Task	N-H 56B-Base	N-H 47B-Base	Qwen-2.5 72B-Base	Llama-3.1 70B-Base	DS-V3 671B-Base	Llama-3.1 405B-Base
General						
MMLU-Pro (5-shot COT)	60.5	61.8	58.8	51.3	<i>64.4</i>	<i>52.8</i>
MMLU (5-shot)	84.2	83.6	86.1	78.8	<i>87.1</i>	<i>84.4</i>
Math						
GSM8k (8-shot COT)	93.7	93.3	90.9	83.9	<i>89.3</i>	<i>83.5</i>
MATH (4-shot COT)	59.4	57.4	64.6	42.9	<i>61.6</i>	<i>49.0</i>
MATH Level 5 (4-shot COT)	35.2	34.1	41.2	21.1		
MMLU STEM (5-shot)	80.6	79.8	84.9	70.5		
Code						
HumanEval (0-shot greedy pass@1)	60.4	61.0	56.7	57.3	<i>65.2</i>	<i>54.9</i>
HumanEval+ (0-shot greedy pass@1)	54.3	56.1	50.0	52.4		
MBPP sanitized (3-shot greedy pass@1)	77.8	75.9	78.2	70.0	<i>75.4</i>	<i>68.4</i>
MBPP+ (0-shot greedy pass@1)	67.2	65.6	71.7	66.9		
Commonsense understanding						
Arc-Challenge (25-shot)	95.0	94.6	95.8	93.0	<i>95.3</i>	<i>95.3</i>
Hellaswag (10-shot)	89.0	87.9	87.6	88.1	<i>88.9</i>	<i>89.2</i>
Winogrande (5-shot)	84.5	83.9	84.4	85.6	<i>84.9</i>	<i>85.2</i>
PIQA (0-shot)	85.0	83.9	83.6	84.1	<i>84.7</i>	<i>85.9</i>
OpenbookQA (0-shot)	48.6	48.8	46.2	47.6		
Long-thought reasoning						
MATH (R1-style 4-shot COT)	87.8		73.9	38.7		
MATH Level 5 (R1-style 4-shot COT)	74.8		53.2	16.7		

Table 4 | Accuracy of Nemotron-H-56B-Base (and its distilled version Nemotron-H-47B-Base, discussed in §3) versus existing SoTA models. N-H is short for Nemotron-H, DS is short for DeepSeek. Numbers in italics are from the DeepSeek-V3 report (DeepSeek-AI, 2025b), all other numbers are run by us. We bold the highest accuracy in each row, excluding italicized numbers.

except for ARC-Challenge (Clark et al., 2018), where we present all options at the same time, similar to MMLU (Hendrycks et al., 2021a).

Accuracy results for Nemotron-H-56B-Base and Nemotron-H-8B-Base on common benchmark tasks are shown in Table 4 and Table 5. Nemotron-H-56B-Base and Nemotron-H-47B-Base are both evaluated in FP8, and all other models are evaluated in BF16. Across both model sizes, Nemotron-H base models reach comparable or better accuracy relative to similarly-sized state-of-the-art Transformer models.

We compare Nemotron-H-56B-Base directly with Qwen-2.5-72B-Base (Qwen, 2025) and Llama-3.1-70B-Base (Meta, 2024). Out of the 17 task we evaluate, Nemotron-H-56B-Base achieves the highest accuracy of the three models on 9 tasks, Qwen-2.5-72B-Base achieves the highest accuracy on 7 tasks, and Llama-3.1-70B-Base achieves the highest accuracy on 1 task; Nemotron-H-56B-Base outperforms Llama-3.1-70B-Base on all but that single task (Winogrande). We further compare Nemotron-H-56B-Base with two much larger state-of-the-art models, DeepSeek-V3-671B-Base (DeepSeek-AI, 2025b) and Llama-3.1-405B-Base (Meta, 2024); we use publicly-reported numbers for these two models on the subset of common tasks where numbers are reported. Surprisingly, Nemotron-H-56B-Base remains competitive with these models, outperforming DeepSeek-V3-671B-Base and Llama-3.1-405B-Base on 4 and 5 out of the 10 overlapping tasks respectively.

We observe similar accuracy results for Nemotron-H-8B-Base compared to Qwen-2.5-7B-Base and Llama-3.1-8B-Base (Table 5). Out of the 15 tasks used for evaluation, Nemotron-H-8B-Base, Qwen-

Task	Nemotron-H 8B-Base	Nemotron-T 8B-Base	Qwen-2.5 7B-Base	Llama-3.1 8B-Base	Gemma-3 12B-Base
General					
MMLU-Pro (5-shot COT)	44.0	41.4	48.3	35.9	45.3
MMLU (5-shot)	72.8	73.2	74.2	65.3	<i>74.5</i>
Math					
GSM8k (8-shot COT)	87.1	89.0	83.3	55.5	74.1
MATH (4-shot COT)	46.5	46.7	49.8	19.5	42.1
MATH Level 5 (4-shot COT)	22.9	25.8	24.6	5.6	17.5
MMLU STEM (5-shot)	65.4	65.6	71.2	56.3	
Code					
HumanEval (0-shot greedy pass@1)	58.5	59.8	56.7	37.8	46.3
HumanEval+ (0-shot greedy pass@1)	55.5	53.0	48.8	31.7	34.1
MBPP sanitized (3-shot greedy pass@1)	65.4	63.4	69.3	57.2	64.6
MBPP+ (0-shot greedy pass@1)	59.5	61.4	65.3	51.6	59.0
Commonsense understanding					
Arc-Challenge (25-shot)	88.7	88.3	89.2	80.4	
Hellaswag (10-shot)	83.2	82.5	80.3	82.3	<i>84.2</i>
Winogrande (5-shot)	80.5	78.8	76.1	78.1	<i>74.3</i>
PIQA (0-shot)	82.2	82.0	80.1	81.0	<i>81.8</i>
OpenbookQA (0-shot)	47.2	44.8	47.0	45.4	

Table 5 | Accuracy of Nemotron-H-8B-Base versus existing SoTA models and a Transformer (Nemotron-T-8B-Base) trained on exactly the same data. Likelihood-based evaluations of the Gemma 3 model are based on the Gemma 3 report (DeepMind, 2025), all other numbers are run by us. We bold the highest accuracy in each row, excluding italicized numbers.

2.5-7B-Base, and Llama-3.1-8B-Base achieve the highest accuracy of the three models on 7, 8, and 0 tasks respectively. Nemotron-H-8B-Base is particularly strong on commonsense understanding tasks, achieving the highest accuracy on 4 out of 5 tasks in this category. As above, we also include comparisons to a larger model, Gemma-3-12B-Base (DeepMind, 2025); Nemotron-H-8B-Base is competitive with the larger model.

Table 5 additionally includes the largest apples-to-apples comparison of a hybrid Mamba-Transformer and pure Transformer model to date (Nemotron-H-8B-Base versus Nemotron-T-8B-Base). Nemotron-H-8B-Base reaches higher accuracy than the Transformer trained on exactly the same data on 7 out of 15 tasks, and is within one point on an additional 4 tasks. Overall, this experiment shows that hybrid models can reach equal or better accuracy compared to Transformer models when trained at state-of-the-art scales.

2.6. Inference Speed

Due to the reduction in self-attention layers, Nemotron-H-8B/56B-Base provide inference-time speedups compared to the alternative Transformer models in Tables 4 and 5 above. To quantify these speedups, we plot the MMLU-Pro accuracy versus inference throughput for Nemotron-H-56B-Base and similarly-sized Transformer models in Figure 1 and for Nemotron-H-8B-Base and relevant baselines in Figure 7. We use an input sequence length of 65536 and ask the models to generate 1024 output tokens. We use an initial Megatron-LM implementation for Nemotron-H inference and vLLM v0.7.3¹² for baselines. In these experiments, we try to maximize per-GPU inference throughput by using as large a batch size as possible, and we run all experiments on NVIDIA H100 GPUs. We

¹²<https://github.com/vllm-project/vllm/tree/v0.7.3>.

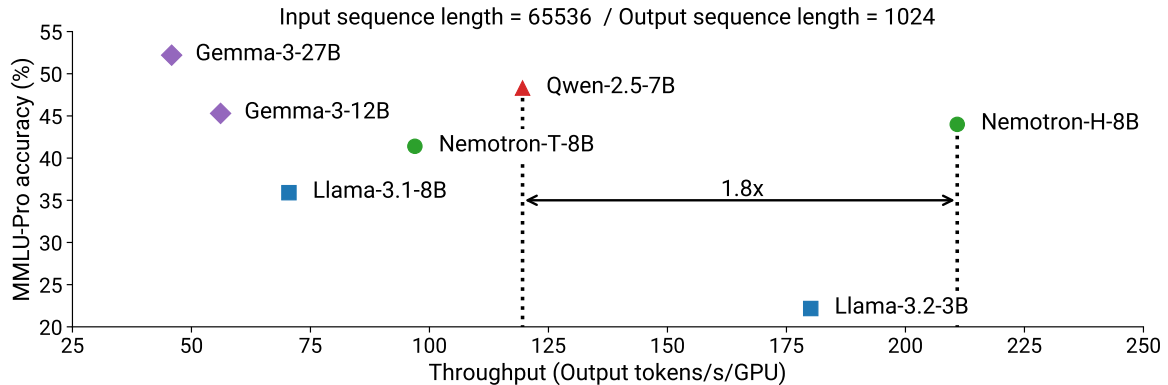


Figure 7 | MMLU-Pro accuracy versus inference throughput (normalized by number of GPUs used) for Nemotron-H-8B-Base compared to existing similarly-sized Transformer models.

report results normalized by the number of GPUs used (i.e., output tokens per second per GPU).

In the setting described above, Nemotron-H-56B-Base can generate $2.4\times$ more output tokens per second per GPU compared to Qwen-2.5-72B and Llama-3.1-70B (and $2.9\times$ more after distillation to Nemotron-H-47B-Base, see §3). Compared to Llama-3.1-405B, Nemotron-H-56B-Base achieves $19.6\times$ higher throughput. Similar to the larger models, Nemotron-H-8B-Base is also faster to infer than corresponding Transformer models. As shown in Figure 7, on longer contexts, we measure a $1.8\times$ and $3\times$ speedup compared to Qwen-2.5-7B and Llama-3.1-8B. Inference speedups are a byproduct of two factors: a) constant computation in the Mamba-2 layers as opposed to linear computation in self-attention layers, b) lower memory footprint from Mamba-2 layers facilitates using higher batch sizes, increasing efficiency. We expect further optimizing Nemotron-H inference to lead to additional speedups compared to Transformers, which have been heavily optimized over the last couple of years.

3. Compression and Distillation

Efficient deployment of LLMs often requires tailoring the model architecture to specific constraints imposed by hardware. In this section, we describe the pruning and distillation process used to compress the 56B model to 47B parameters with the goal of running longer context inference on the NVIDIA GeForce RTX 5090 GPU (storing the weights of a 56B parameter model in FP4 precision on a RTX 5090 GPU with 32GiB of memory will require 29.5GiB, leaving only 2.5GiB for KV cache and activation buffers). We introduce a novel model compression framework called MiniPuzzle that combines the simplicity of Minitron (Sreenivas et al., 2024; Muralidharan et al., 2024) with the versatility of Puzzle (Bercovich et al., 2024). Our approach uses roughly $300\times$ fewer tokens to obtain a 47B model compared to training from scratch. Our compressed 47B model achieves a $1.2\times$ inference speedup (Figure 1) while achieving accuracy on par with the original 56B model.

3.1. MiniPuzzle Overview

MiniPuzzle combines lightweight pruning with neural architecture search (NAS) to produce efficient compressed models that meet specific target deployment constraints. Figure 8 provides a high-level overview of the framework. MiniPuzzle’s optimization process consists of three stages: a) importance estimation (§3.2), b) conditional NAS (§3.3), and c) knowledge distillation (§3.4).

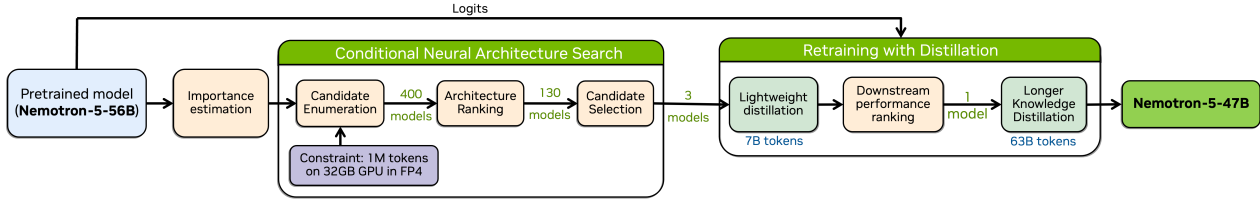


Figure 8 | MiniPuzzle’s optimization process: a) estimate layer and FFN importance scores, b) search for the best model candidates using the conditional Neural Architecture Search (NAS) framework, considering the 32GiB GPU memory constraint, c) select the best candidate with lightweight distillation and recover the accuracy lost due to pruning with longer distillation.

3.2. Importance Estimation

MiniPuzzle first collects importance or sensitivity scores for each model component (e.g., layers, FFN neurons) to help decide which components to remove; this is the *importance estimation* phase. The scores computed in this phase are used to decide which model components can be pruned. We note that sensitivity analysis based on gradient information is typically impractical at modern LLM scale (Muralidharan et al., 2024); instead, we rely on a lightweight strategy that uses only on forward passes. In this work, we use a simplified approach that works well in our ablation studies: a) prune layers, and b) prune FFN hidden dimensions (effectively neurons). We also experimented with pruning Mamba heads and Mamba head dimension; unfortunately, both axes caused severe accuracy degradation (particularly head dimension pruning).

We now describe how we compute the importance of each layer and FFN neuron.

Layer importance. We use the scoring method from Puzzle to estimate the importance of each layer in the model. Given an input tensor, layer importance is computed as the Mean Squared Error (MSE) between the intermediate activation tensor just before the LM head of the full model and the same activation tensor for a model with the particular layer removed. We average these rankings over a small random subset of the training data (128 samples in our case) to obtain a reliable estimate of importance that takes into account sample variability.

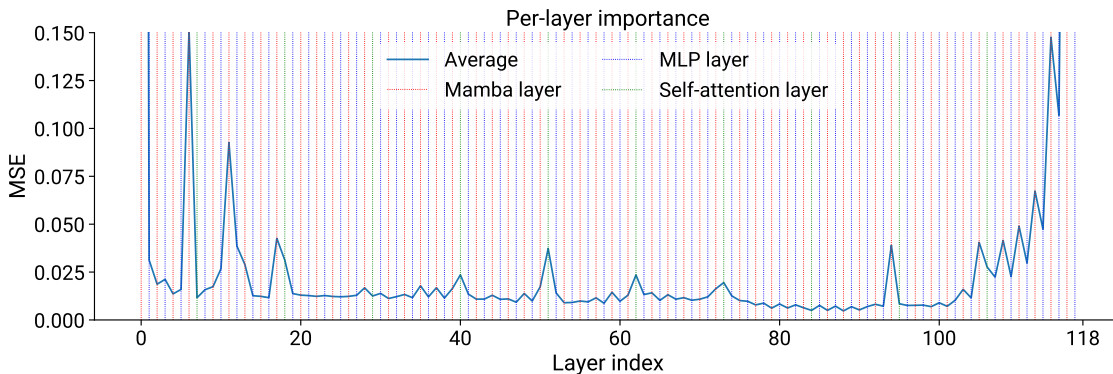


Figure 9 | Layer importance measured as the MSE between the full model and a model with that layer removed, averaged over a small training subset. Vertical dotted lines indicate layer types: self-attention (green), FFN (blue), and Mamba-2 (red).

Figure 9 plots average importance scores of each layer in Nemotron-H-56B-Base. The green, blue and red dotted lines correspond to self-attention, FFN and Mamba layers. We notice from the figure

that the 56B model follows a typical pattern observed in Minitron: the most important layers are concentrated at the beginning and end of the model. Additionally, MSE importance reveals that even though the 56B model only has 10 self-attention layers, some self-attention layers are ranked among the least important, particularly the 84th (7th self-attention layer). However, layers 40, 51, 62 and 73 seem to be more important compared to the other layers in their immediate vicinity.

FFN importance. FFN layers internally are composed of two linear operators with a non-linear activation in between:

$$\text{FFN}(\mathbf{X}) = \delta\left(\mathbf{X} \cdot \mathbf{W}_1^T\right) \cdot \mathbf{W}_2.$$

Here, \mathbf{X} denotes the input, and \mathbf{W}_1 and \mathbf{W}_2 are the two associated weight matrices in the FFN layer. $\mathbf{W}_1, \mathbf{W}_2 \in \mathbb{R}^{d_{ffn} \times d_{model}}$, where d_{model} and d_{ffn} are the model hidden dimension and FFN hidden dimension respectively (Table 1). $\delta(\cdot)$ refers to the non-linear activation function (squared ReLU in this work).

Following the same procedure as Minitron, we compute the importance of each neuron in the first linear operator of each FFN layer by examining the set of outputs it produces. We use a small calibration dataset of 1024 samples for this purpose. Formally, we compute each neuron’s importance score by aggregating its outputs given an input batch X :

$$F_{\text{neuron}}^{(i)} = \sum_{\mathbf{B}, \mathbf{S}} \delta\left(\mathbf{X}(\mathbf{W}_1^i)^T\right).$$

Here, \mathbf{W}_1^i refers to the i^{th} row of the weight matrix \mathbf{W}_1 . $\sum_{\mathbf{B}, \mathbf{S}}$ refers to aggregation along the batch and sequence dimensions. We use the `mean` and `l2-norm` aggregation functions along the batch and sequence dimensions, following the observations in the Minitron paper (Muralidharan et al., 2024). For a sequence of scores \mathbf{S} , `mean` aggregation is defined as $\frac{1}{n} \sum_{i=1}^n |\mathbf{S}_i|$, and `l2-norm` is $\sqrt{\sum_{i=1}^n \mathbf{S}_i^2}$.

3.3. Conditional NAS

MiniPuzzle’s conditional NAS utilizes the importance scores of every layer and FFN neuron (computed as described in §3.2) to identify architectures that meet memory constraints while preserving the most critical components. This process allows us to efficiently explore the vast search space of possible layer configurations, and consists of three steps:

1. **Pruned candidate enumeration.** We iterate over a grid of possible layer counts for each layer type (i.e., number of self-attention, FFN, and Mamba-2 layers), and FFN hidden dimension (24576, 25600, ..., 32768). For each target layer count and FFN hidden dimension size, we select the top layers and neurons based on their respective importance scores (see §3.2 for details on importance estimation) and realize the corresponding architecture; i.e., we drop the irrelevant layers and prune all FFN layers to the same target width. Only architectures that meet the target memory constraint of less than 31.7 GiB (computed as the total memory required for FP4 inference on a context of size 1 million tokens) are retained, resulting in around 400 candidate architectures.
2. **Architecture ranking.** We score the candidate architectures using a lightweight metric that compares them to the parent model (Nemotron-H-56B-Base) on a small validation corpus with 1 million tokens. Specifically, we use two different scores to estimate the quality of each candidate model: a) next-token accuracy which computes how often the child model correctly predicts the next ground-truth token, and b) next-token parent agreement which computes

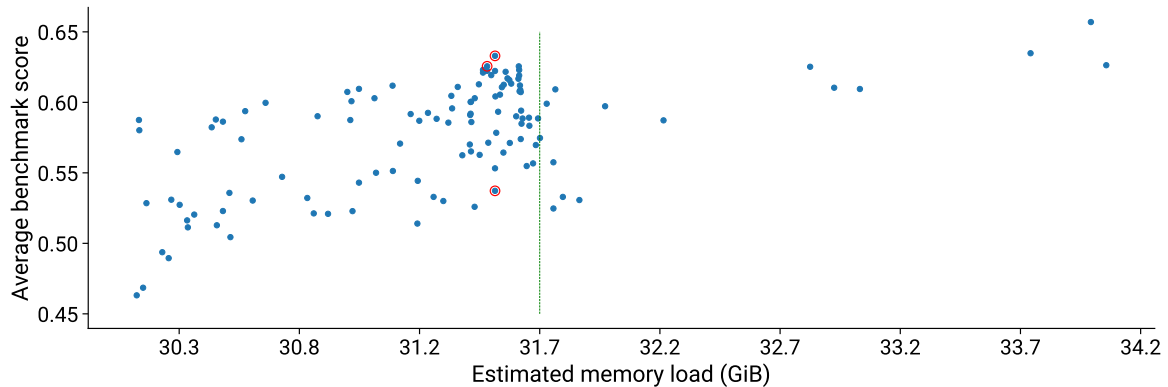


Figure 10 | Average benchmark score for pruned candidates with different memory budgets. Each dot represents a different candidate, i.e., model with different set of layers pruned with respect to how much memory it consumes. The green dotted line marks the upper memory limit we consider and the dots marked with red circles are the candidates selected for further distillation.

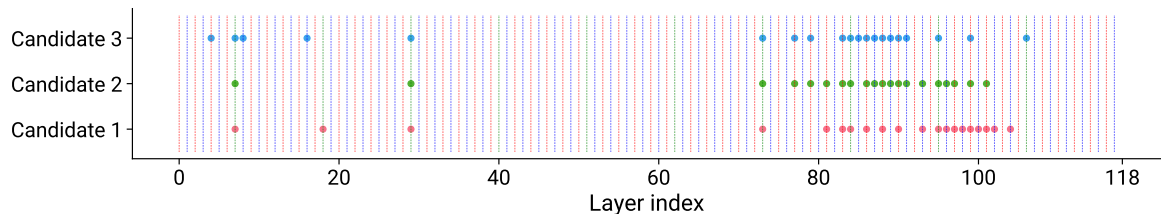


Figure 11 | Pruned layers for the top three candidates. Each row represents a candidate, with dots indicating dropped layers. Vertical dotted lines denote layer types: green for self-attention, blue for FFN, and red for Mamba.

how often the child model agrees with the parent model about the greedy prediction of the next token. We rank all candidate architectures using both scoring metrics, and retain the top 130 performers.

- Candidate selection.** We now refine the set of ranked architectures from 130 to a manageable 3 by benchmarking them on a subset of evaluation tasks. The first column of Table 6 lists the tasks we use to evaluate the final 3 candidates. We use the average scores across all these tasks for evaluation. Figure 10 plots the average benchmark scores for all 130 candidates, and Figure 11 illustrates the specific layers dropped by all three candidates. Candidates 1 and 2 achieve the highest benchmark scores and drop similar layers. Candidate 3, which drops a slightly different set of layers, performs significantly worse after pruning. However, we include it here to study the extent to which distillation can compensate for the loss.

3.4. Retraining with Distillation

To recover the accuracy lost due to pruning, the model undergoes continued training. Recent work has demonstrated that distilling knowledge from the original model to the pruned model outperforms conventional fine-tuning (as shown in Minitron and Puzzle); we thus adopt logit-based distillation for continued training, employing forward KL divergence loss exclusively during the accuracy recovery phase (see §3 of the Minitron paper for more details on the distillation loss formulation).

Following the initial candidate selection process described in §3.3, we perform short distillation of

Benchmark	Nemotron-H 56B-Base	Candidate 1 47B-pruned	Candidate 2 47B-pruned	Candidate 3 47B-pruned
MMLU	84.2	81.5 → 83.7	80.8 → 83.2	81.3 → 83.6
Commonsense understanding (average)	67.6	64.2 → 66.6	63.8 → 67.2	64.5 → 66.8
GSM8k	91.4	67.9 → 89.2	60.7 → 91.1	19.5 → 90.5
Code (average)	67.0	52.0 → 64.9	52.7 → 64.6	23.0 → 64.9
AVERAGE	70.6	63.3 → 69.3	62.1 → 69.6	53.7 → 69.5

Table 6 | Comparison of benchmark scores for pruned candidates before and after lightweight distillation. Scores might be slightly different to those presented in Table 4 due to minor differences in evaluation settings and averages over different sets of tasks.

the top 3 candidates using ~ 7 B tokens, with the 56B model as the teacher. We observe from our experiments that this step is crucial for picking the best possible final candidate. Table 6 details the benchmark scores for the 3 candidates before and after short distillation. The most accurate candidate (averaged across all benchmarks) of the three is chosen for an extended distillation run using 63 billion tokens to produce the final 47B model; in our case, Candidate 2 performs best, as shown in Table 6. We observe that the choice of the final candidate varies based on the ultimate objective; for instance, prioritizing accuracy in coding tasks versus commonsense reasoning tasks.

All distillation runs use FP8 precision, a softmax temperature of 1.0, which controls the softness of the probability distribution during knowledge distillation (Hinton et al., 2015), sequence length of 8192, and a batch size of 768 samples.

3.5. Results

Using the MiniPuzzle approach, we efficiently compress the 56B model to 47B parameters by pruning full layers (depth) and FFN hidden dimension size, improving inference speed and enabling longer-context inference on a 32GiB NVIDIA GeForce RTX 5090 GPU. The 47B model retains half the self-attention layers of 56B (5 instead of 10), along with 44 Mamba-2 layers (down from 54) and 49 FFN layers (down from 54). Additionally, the FFN intermediate size was pruned from 32768 to 30720. As shown in Figure 1 and Table 4, the resulting 47B model achieves a $1.2\times$ faster inference on long contexts and near-lossless accuracy on benchmarks while requiring roughly $300\times$ fewer tokens compared to training from scratch.

4. Vision-Language Models

In this section, we introduce Nemotron-H-8B-VLM and Nemotron-H-56B-VLM, which are built on Nemotron-H-8B-Instruct and Nemotron-H-56B-Base. Vision-Language Models (VLMs) are generally recommended to be built on aligned models to enhance instruction-following capabilities (Dai et al., 2024). In this work, we chose to build Nemotron-H-8B-VLM and Nemotron-H-56B-VLM on Nemotron-H-8B-Instruct and Nemotron-H-56B-Base (since Nemotron-H-56B-Instruct was unavailable). Both Nemotron-H-8B-VLM and Nemotron-H-56B-VLM have been used as the base models for building Cosmos-Reason1 (NVIDIA et al., 2025), a family of frontier reasoning models for physical AI.

4.1. Model Architecture

In previous studies, VLMs were constructed by integrating a text-only LLM with a vision encoder. Two prevalent architectures for this integration are the decoder-only architecture (Liu et al., 2023a)

and the cross-attention-based architecture (Alayrac et al., 2022). We use the decoder-only NVLM-D architecture (Dai et al., 2024) due to its simplicity, parameter efficiency, ability to process high-resolution image inputs, and unified handling of multiple modalities by mapping non-text tokens (e.g., images, audio, videos) into the same embedding space as text tokens. Nemotron-H-VLM comprises a vision encoder, a projector (a two-layer FFN), and the Nemotron-H LLM backbone.

Vision encoder. For both the 8B and 56B VLMs, we use InternViT-300M-V2.5 (Chen et al., 2024) as the vision encoder. It processes static 448×448 pixel images as input with patch size 14×14 , and generates 1024 visual tokens in total. Each visual token is represented by a 1024-dimensional vector. Following the NVLM design (Dai et al., 2024), we dynamically resize the input image to the closest predefined aspect ratio $\{a : b\}$ (a and b are integers) based on its resolution and segment it into $a \times b \leq 12$ tiles¹³, each corresponding to a 448×448 -pixel image tile. To preserve global context, we also generate a thumbnail 448×448 tile, which is a scaled-down version of the whole image. For example, given a 1920×1080 image, the closest predefined aspect ratio is $3 : 2$. The image is resized to 1344×896 and divided into $3 \times 2 + 1 = 7$ tiles, including one thumbnail tile.

To reduce processing overhead for the LLM, we downsample 1024 tokens to 256 by grouping four neighboring image tokens and concatenating them along the channel dimension. The image tokens from multiple tiles are concatenated with an interleaved tile ID tag in raw text format, which gives the downstream LLM information about the dynamic tiling structure; we find this is crucial to improving accuracies on various vision-language benchmarks. For more details, see the NVLM technical report (Dai et al., 2024). The concatenated visual tokens are processed by a two-layer FFN block, which maps each visual token into the text token embedding space. These embeddings are then fed into the LLM backbone.

4.2. Training Method and Data

Following NVLM (Dai et al., 2024), Nemotron-H-VLM is trained in two stages:

1. **VL pre-training.** We train only the two-layer FFN for modality alignment while keeping both the Nemotron-H backbone and vision encoder frozen.
2. **VL SFT.** We fine-tune the vision encoder, FFN projector, and Nemotron-H backbone end-to-end on various task-oriented SFT data.

For VL pre-training, we utilize a large and diverse image-text pre-training dataset from NVLM (Dai et al., 2024), including captioning (Lin et al., 2015; Sharma et al., 2018; Ordonez et al., 2011; Li et al., 2022), visual question answering (VQA) on natural image (Goyal et al., 2017; Krishna et al., 2017), visual chart (Kafle et al., 2018) and document understanding (Marafioti & Laurencon, 2024), optical character recognition (OCR) (Mishra et al., 2019) and scene-text recognition (Veit et al., 2016), and visual math reasoning (Lindström & Abraham, 2022) data. Overall, our VL pre-training dataset consists of 130 million samples. We apply careful sanitization to remove any potentially harmful content.

For VL SFT, we leverage diverse and high-quality datasets from NVLM (Dai et al., 2024) and Eagle2 (Li et al., 2025). In addition to the previously mentioned categories, the dataset also includes knowledge-based VQA (Marino et al., 2019), visual reasoning (Hudson & Manning, 2019), science-

¹³The predefined ratios are $\{a : b\} = \{1 : 1, 1 : 2, 1 : 3, 1 : 4, 1 : 5, 1 : 6, 1 : 7, 1 : 8, 1 : 9, 1 : 10, 1 : 11, 1 : 2, 2 : 1, 2 : 2, 2 : 3, 2 : 4, 2 : 5, 2 : 6, 3 : 1, 3 : 2, 3 : 3, 3 : 4, 4 : 1, 4 : 2, 4 : 3, 5 : 1, 5 : 2, 6 : 1, 6 : 2, 7 : 1, 8 : 1, 9 : 1, 10 : 1, 11 : 1, 12 : 1\}$.

Task	Nemotron-H 8B-VLM	VLM w/ Llama3.1 8B-Instruct	VLM w/ Qwen2.5 7B-Instruct
MMMU (val)	51.3	44.8	51.1
MathVista	62.5	61.7	63.8
ChartQA	84.8	85.4	84.9
AI2D	89.6	90.9	91.0
OCRBench	840	847	836
TextVQA	76.2	76.4	76.1
RealWorldQA	62.2	60.9	60.6
DocVQA	90.6	91.3	91.2

Table 7 | Evaluation of Nemotron-H-8B-VLM on vision-language benchmarks. We compare to the VLMs built with Llama-3.1-8B-Instruct and Qwen2.5-7B-Instruct using the same training recipe.

Task	Nemotron-H 56B-VLM	VLM w/ Qwen2.5 72B-Instruct	NVLM-D-1.0 72B (2024-09-17)
MMMU (val)	63.6	65.1	62.6 [†]
MathVista	70.7	70.5	66.7 [†]
ChartQA	89.4	88.9	86.0
AI2D	94.7	94.9	94.2
OCRBench	862	869	853
TextVQA	81.1	83.5	82.1
RealWorldQA	68.4	71.4	69.7
DocVQA	93.2	92.0	92.6

Table 8 | We evaluate Nemotron-H-56B-VLM on a range of vision-language benchmarks, and compare it to a VLM built using Qwen2.5-72B-Instruct with the same training recipe. We also compare with NVLM-1.0-D 72B, a previous state-of-the-art VLM developed by NVIDIA. [†]We evaluate NVLM-1.0-D 72B on MMMU and MathVista using VLMEvalKit (Duan et al., 2024); this is the same evaluation setup used for other models and yields better results than the official numbers.

related VQA (Lu et al., 2022), and visual instruction-following data. Overall, our VL SFT dataset consists of 6 million image-text samples. Dai et al. (2024) and Li et al. (2025) have more details.

4.3. Vision-Language Benchmark Results

We evaluate Nemotron-H-8B-VLM and Nemotron-H-56B-VLM on a comprehensive set of vision-language benchmarks, including MMMU (Yue et al., 2024), MathVista (Lu et al., 2024), ChartQA (Masry et al., 2022), AI2D (Kembhavi et al., 2016), OCRBench (Liu et al., 2024), TextVQA (Singh et al., 2019), RealWorldQA (xAI, 2024), and DocVQA (Mathew et al., 2021). These benchmarks assess a broad range of capabilities such as multimodal reasoning, mathematical reasoning in visual contexts, natural image understanding, scene-text recognition, chart & document understanding, real-world perception, and OCR.

We compare Nemotron-H-8B-VLM with VLMs built on LLaMA-3.1-8B-Instruct and Qwen2.5-7B-Instruct, using the same training methodology and dataset. As shown in Table 7, Nemotron-H-8B proves to be a strong LLM backbone for developing best-in-class VLMs. We further compare Nemotron-H-56B-VLM with NVLM-1.0-D (Dai et al., 2024) and the VLM built with Qwen2.5-72B-Instruct using the same training recipe in Table 8. Nemotron-H-56B-VLM achieves state-of-the-art results, demonstrating superior quality compared to previous models.

5. Alignment and Long Context

Finally, we study the extent to which our hybrid Mamba-Transformer models can be effectively post-trained to produce instruct and long-context variants.

We use the Nemotron-H-8B-Base model as the starting point for this study and conduct instruction-tuning and long-context extension using a pipeline consisting of three stages. In the first stage (**stage1**), we perform supervised fine-tuning (SFT) over a data blend consisting of 6 million code- and math-related prompts and responses, as well as other data with general instruction-following tasks. This data blend is enhanced with long-context dependencies by sampling a small set of (**prompt**, **response**) pairs and synthetically extending them to create longer contexts. Concretely, given a (**prompt**, **response**) pair from the **stage1** dataset, we extend the sample to (**prompt**, **response**, **extended_prompt**, **extended_response**) where **extended_prompt** and **extended_response** are generated using an instruction-tuned model. We repeat this process until the sample reaches the desired length (e.g., 32k tokens) and include these additional long-context examples in the **stage1** dataset for SFT training.

In the second stage (**stage2**), we start with preference tuning on general-domain prompts instead of SFT. For preference optimization, we employ offline RPO (Sun et al., 2025). Following this step, we perform a round of RPO focused on narrow instruction following, similar to the style of prompts and responses in the IFEval Benchmark (Zhou et al., 2023).

In the last stage (**stage3**), we use on-policy RPO, in which both preferred and dis-preffered responses are generated by the **stage2** model checkpoint. For on-policy-RPO, we add additional safety data derived from AEGIS2.0 (Ghosh et al., 2025). We also increase the scale of the rewards used in this stage as we found it resulted in better scores for downstream benchmarks.

To support long contexts, we extend our **stage1** SFT dataset to 512k tokens and (in similar fashion) our off-policy RPO dataset to 32k tokens. We observed that training on longer samples (e.g., 512k tokens) improved RULER (Hsieh et al., 2024) scores on shorter sequence lengths as well (e.g., 128k).

Task	Llama-3.1 8B-Instruct	Qwen2.5 7B-Instruct	Nemotron-H 8B-Instruct
IFEval Prompt	73.2	72.6	74.7
IFEval Instruct	81.2	80.2	82.5
BFCL (V2)	38.9	61.1	62.6
MATH500	47.8	76.4	77.6
MT-Bench	7.49	8.04	7.90
MMLU (0-shot generative)	63.1	70.9	68.7
MBPP	75.1	79.9	81.0
MBPP+	61.9	67.5	67.7
HumanEval	69.5	82.3	79.3
HumanEval+	64.0	75.6	74.4
GSM8K	81.6	89.8	90.4

Table 9 | Comparison of benchmarks after post-training across Llama-3.1-8B-Instruct, Qwen2.5-7B-Instruct, and Nemotron-H-8B-Instruct.

We conduct a thorough evaluation of the final aligned checkpoint across a diverse set of benchmarks, and compare to Llama-3.1-8B-Instruct and Qwen-2.5-7B-Instruct (Meta, 2024; Qwen, 2025). Table 9 shows Nemotron-H-8B-Instruct to be competitive with state-of-the-art instruction-tuned Transformer models. We also use the RULER benchmark (Hsieh et al., 2024) to evaluate each of the three model’s long-context capabilities (Table 10). Despite having only four self-attention layers, Nemotron-H-8B-

Context length	Llama-3.1 8B-Instruct	Qwen2.5 7B-Instruct	Nemotron-H 8B-Instruct
16,384	91.6	93.0	91.5
32,768	87.4	91.1	89.8
65,536	84.7	90.4	87.6
131,072	77.7	84.4	81.7

Table 10 | Comparison of RULER scores across sequence lengths between Llama-3.1-8B-Instruct, Qwen2.5-7B-Instruct, and Nemotron-H-8B-Instruct.

Instruct is competitive with these models on the RULER long-context benchmark.

Comparison to Transformer model alignment. The above results are consistent with our internal ablations comparing post-training of Transformer and hybrid Mamba-Transformer models pre-trained in similar ways.

Before developing Nemotron-H-8B-Instruct, we conducted smaller-scale post-training experiments on a Transformer (Nemotron-T-8B-Exp-Base) and hybrid model (Nemotron-H-8B-Exp-Base) pre-trained on identical datasets. Table 11 shows the accuracies of these two base models across selected benchmarks involving math, code, and general knowledge tasks. As for the final Nemotron-H-8B-Base and Nemotron-T-8B-Base models in Table 5, both experimental models reach comparable accuracy.

Task	Nemotron-T 8B-Exp-Base	Nemotron-H 8B-Exp-Base
MMLU (5-shot)	70.3	69.9
GSM8k	64.8	64.1
MBPP+ (0-shot greedy pass@1)	53.7	54.5
PIQA (0-shot)	81.1	82.8
OpenBookQA (0-shot)	45.4	46.2

Table 11 | Comparison of experimental Transformer and hybrid base models on various tasks.

We post-trained Nemotron-T-8B-Exp-Base and Nemotron-H-8B-Exp-Base to obtain corresponding instruction-tuned models, Nemotron-T-8B-Exp-Instruct and Nemotron-H-8B-Exp-Instruct. Both models were post-trained using a multi-stage pipeline similar to the one described above for Nemotron-H-8B-Instruct. More specifically, we used:

- Initial supervised fine-tuning (SFT), focusing on code and math (20 million samples), as well as general instruction-following tasks (200k examples).
- Subsequent preference optimization using a dataset of 200k paired comparisons.

For preference optimization, we experimented with using multiple rounds of iterative offline RPO and multiple rounds of iterative DPO. Overall, we observed the two methods to be similar, with marginal differences between them. For the comparison in this section, we select the best final model amongst all candidate models produced through RPO or DPO; the best Nemotron-T-8B-Exp-Instruct model was produced using three rounds of iterative offline RPO and the best Nemotron-H-8B-Exp-Instruct model was produced using two rounds of iterative DPO.

We compare Nemotron-H-8B-Exp-Instruct and Nemotron-T-8B-Exp-Instruct on key alignment benchmarks in Table 12. Across these benchmarks, both models achieved comparable results.

Benchmark	Nemotron-T	Nemotron-H
	8B-Exp-Instruct	8B-Exp-Instruct
MT-Bench	7.9	8.0
MMLU (0-shot generative)	68.0	67.4
MBPP+	65.6	66.9
MATH	68.8	68.5
IFEval Prompt	74.3	74.7
IFEval Instruct	81.8	82.1
BFCL (V2)	64.3	65.4

Table 12 | Comparison of experimental aligned models on key alignment benchmarks.

We also observed similar long-context capabilities for the two models, with both models reaching comparable RULER scores for context lengths of 131,072. These ablation experiments provide additional evidence that hybrid Mamba-Transformer models can be post-trained to yield instruction-tuned models that are on-par or better when compared to equivalent Transformer models.

6. Conclusions

The Nemotron-H family of models demonstrates that hybrid model architectures can offer the best of both worlds: comparable to state-of-the-art Transformer models in terms of capabilities while offering improved inference speed. We find the Nemotron-H base models offer either better or on-par accuracy compared to other similarly-sized state-of-the-art open-sourced Transformer models (e.g., Qwen-2.5-7B/72B and Llama-3.1-8B/70B), while being up to $3\times$ faster at inference. We also find these base models can be adapted to yield effective VLMs as well as instruction-tuned models. Additionally, both our FP8-based training recipe and MiniPuzzle can be used to reduce the cost of creating these models.

We will be releasing the Nemotron-H family of models described in this paper (along with instruct and reasoning models based off of Nemotron-H-47B-Base) with support in Hugging Face, NeMo, and Megatron-LM to facilitate further research.

Contributors

We thank the following people for their invaluable contributions to Nemotron-H.

Data. Abhinav Khattar, Aleksander Ficek, Amala Sanjay Deshmukh, Andrew Tao, Ayush Dattagupta, Brandon Norick*, Chengyu Dong*, Dan Su*, Daria Gitman, Evelina Bakhturina, Igor Gitman, Ilia Karmanov, Ivan Moshkov, Jane Polak Scowcroft, Jarno Seppanen, Jiaxuan You, Jocelyn Huang, John Kamalu*, Joseph Jennings*, Jupinder Parmar*, Karan Sapra, Kateryna Chumachenko, Kezhi Kong*, Lukas Voegtle, Lindsey Pavao, Markus Kliegl*, Matvei Novikov, Mehrzad Samadi, Miguel Martinez, Mostofa Patwary*, Osvald Nitski, Philipp Fischer, Pritam Gundecha, Rabeeh Karimi, Sean Narenthiran, Sanjeev Satheesh*, Seungju Han, Shrimai Prabhumoye*, Shubham Pachori, Shubham Toshniwal, Siddhartha Jain, Somshubra Majumdar, Syeda Nahida Akter*, Timo Roman, Ushnish De, Vahid Noroozi, Vitaly Kurin, Wasi Uddin Ahmad, Wei Du, Yao Xu, Yejin Choi, Ying Lin*.

FP8 recipe. Carlo del Mundo, Dusan Stosic, Eric Chung, Jinze Xue, John Kamalu, Kirthi Sivamani, Mike Chrzanowski*, Mohammad Shoeybi, Mostofa Patwary, Oleg Rybakov*, Paulius Micikevicius, Peter Dykas*, Przemek Tredak, Zhongbo Zhu.

Model architecture. Brandon Norick*, Duncan Riach*, Roger Waleffe*, Wonmin Byeon*.

Pre-training. Deepak Narayanan*, Hongbin Liu, Kunlun Li, Maciej Bala, Michael Andersch, Mikolaj Blaz, Oleg Rybakov, Peter Dykas, Roger Waleffe*, Sangkug Lym, Selvaraj Anandaraj, Seonmyeong Bak, Slawek Kierat, Szymon Migacz, Xiaowei Ren.

Infrastructure. Aaron Blakeman, Aarti Basant, Ashwin Poojary, Brian Butterfield, Christine Harvey, Ding Ma, Dong Ahn, Gargi Prasad, Hui Li, Jason Sewall, Jing Zhang, Jining Huang, Kumar Anik, Maer Rodrigues de Melo, Mohamed Fawzy, Ning Xu, Pasha Shamis, Pierre-Yves Aquilanti, Rahul Kandu, Ruoxi Zhang, Sabrina Kavanaugh, Sergey Kashirsky, Shelby Thomas, Sirshak Das, Sriharsha Niverty, Stefania Alborghetti, Tal Shiri.

Distillation. Akhiad Bercovich*, Ali Taghibakhshi*, Daniel Korzekwa, Elad Segal*, Izik Golan*, Marcin Chochowski*, Mostofa Patwary, Pavlo Molchanov*, Ran El-Yaniv, Raviraj Joshi, Roger Waleffe, Saurav Muralidharan*, Sharath Turuvekere Sreenivas*, Tomer Ronen*.

VLM. Andrew Tao, Boxin Wang*, Danny Yin, Fuxiao Liu, Guilin Liu, Guo Chen, Jason Lu, Jon Barker, Lukas Voegtle, Matthieu Le, Mike Ranzinger, Nayeon Lee*, Philipp Fischer, Song Han, Tuomas Rintamaki, Tyler Poon, Wei Ping*, Wenliang Dai*, Zhiding Yu, Zhiqi Li, Zhuolin Yang*.

Alignment and long context. Adithya Renduchintala*, Ali Taghibakhshi*, Ameya Sunil Mahabaleshwarkar, Dima Rekesh*, Ellie Evans, Fei Jia, Gerald Shen*, Haifeng Qian*, Jiaqi Zeng*, Makesh Narsimhan Sreedhar, Michael Evans, Olivier Delalleau*, Prasoon Varshney, Samuel Krیمان*, Shantanu Acharya*, Soumye Singhal, Tugrul Konuk*, Yian Zhang*, Yoshi Suhara*, Zijia Chen.

Inference. Helen Ngo*, Keshav Santhanam*, Vijay Korthikanti*.

Software support. Adithya Renduchintala, Ali Taghibakhshi, Anna Shors, Ashwath Aithal, Balaram Buddharaju, Bobby Chen, Deepak Narayanan, Dmytro Pykhtar, Duncan Riach, Gerald Shen, Helen Ngo, Jared Casper, Jimmy Zhang, Keshav Santhanam, Lawrence McAfee, Luis Vega, Nima Tajbakhsh, Parth Chadha, Piotr Bialecki, Roger Waleffe, Sahil Jain, Terry Kong, Tyler Poon, Vijay Korthikanti, Yoshi Suhara, Zhiyu Li.

Evaluations and safety. Ameya Sunil Mahabaleshwarkar*, Christopher Parisien, David Mosalanezhad, Denys Fridman, Eileen Long, Erick Galinkin, Ewa Dobrowolska, Katherine Luna, Leon Derczynski, Marta Stepniewska-Dziubinska, Michael Evans, Roger Waleffe*, Sanjeev Satheesh*, Shaona Ghosh, Shrimai Prabhumoye, Suseella Panguluri, Syeda Nahida Akter, Varun Singh.

Program management. Joey Conway, Krzysztof Pawelec, Shyamala Prayaga, Swetha Bhendigeri, Trisha Saar.

Leadership. Alexis Bjorlin, Andrew Tao*, Boris Ginsburg*, Bryan Catanzaro*, Eric Chung, Jan Kautz, Jonathan Cohen*, Kari Briski, Misha Smelyanskiy, Mohammad Shoeybi*, Mostofa Patwary*, Oleksii Kuchaiev*, Sharon Clay, Song Han, Timo Roman, Wei Ping*.

* Core contributor.

References

- Joshua Ainslie, James Lee-Thorp, Michiel de Jong, Yury Zemlyanskiy, Federico Lebrón, and Sumit Sanghai. GQA: Training Generalized Multi-Query Transformer Models from Multi-Head Checkpoints, 2023. URL <https://arxiv.org/abs/2305.13245>.
- Syeda Nahida Akter, Shrimai Prabhumoye, John Kamalu, Sanjeev Satheesh, Eric Nyberg, Mostofa Patwary, Mohammad Shoeybi, and Bryan Catanzaro. MIND: Math Informed syNthetic Dialogues for Pretraining LLMs, 2024. URL <https://arxiv.org/abs/2410.12881>.
- Jean-Baptiste Alayrac, Jeff Donahue, Pauline Luc, Antoine Miech, Iain Barr, Yana Hasson, Karel Lenc, Arthur Mensch, Katherine Millican, Malcolm Reynolds, et al. Flamingo: A Visual Language Model for Few-shot Learning. *Advances in Neural Information Processing Systems*, 35:23716–23736, 2022.
- Loubna Ben Allal, Anton Lozhkov, Elie Bakouch, Gabriel Martín Blázquez, Guilherme Penedo, Lewis Tunstall, Andrés Marafioti, Hynek Kydlíček, Agustín Piqueres Lajarín, Vaibhav Srivastav, Joshua Lochner, Caleb Fahlgren, Xuan-Son Nguyen, Clémentine Fourier, Ben Burtenshaw, Hugo Larcher, Haojun Zhao, Cyril Zakka, Mathieu Morlon, Colin Raffel, Leandro von Werra, and Thomas Wolf. SmolLM2: When Smol Goes Big – Data-Centric Training of a Small Language Model, 2025. URL <https://arxiv.org/abs/2502.02737>.
- Zeyuan Allen-Zhu and Yuanzhi Li. Physics of Language Models: Part 3.2, Knowledge Manipulation, 2024. URL <https://arxiv.org/abs/2309.14402>.
- Jacob Austin, Augustus Odena, Maxwell Nye, Maarten Bosma, Henryk Michalewski, David Dohan, Ellen Jiang, Carrie Cai, Michael Terry, Quoc Le, and Charles Sutton. Program Synthesis with Large Language Models, 2021. URL <https://arxiv.org/abs/2108.07732>.
- Iz Beltagy, Matthew E. Peters, and Arman Cohan. Longformer: The Long-Document Transformer, 2020. URL <https://arxiv.org/abs/2004.05150>.
- Akhiad Bercovich, Tomer Ronen, Talor Abramovich, Nir Ailon, Nave Assaf, Mohammad Dabbah, Ido Galil, Amnon Geifman, Yonatan Geifman, Izhak Golan, Netanel Haber, Ehud Karpas, Roi Koren, Itay Levy, Pavlo Molchanov, Shahar Mor, Zach Moshe, Najeeb Nabwani, Omri Puny, Ran Rubin, Itamar Schen, Ido Shahaf, Oren Tropp, Omer Ullman Argov, Ran Zilberstein, and Ran El-Yaniv. Puzzle: Distillation-Based NAS for Inference-Optimized LLMs, 2024. URL <https://arxiv.org/abs/2411.19146>.
- Yonatan Bisk, Rowan Zellers, Ronan Le Bras, Jianfeng Gao, and Yejin Choi. PIQA: Reasoning about Physical Commonsense in Natural Language, 2019. URL <https://arxiv.org/abs/1911.11641>.
- Tom B. Brown, Benjamin Mann, Nick Ryder, Melanie Subbiah, Jared Kaplan, Prafulla Dhariwal, Arvind Neelakantan, Pranav Shyam, Girish Sastry, Amanda Askell, Sandhini Agarwal, Ariel Herbert-Voss, Gretchen Krueger, Tom Henighan, Rewon Child, Aditya Ramesh, Daniel M. Ziegler, Jeffrey Wu, Clemens Winter, Christopher Hesse, Mark Chen, Eric Sigler, Mateusz Litwin, Scott Gray, Benjamin Chess, Jack Clark, Christopher Berner, Sam McCandlish, Alec Radford, Ilya Sutskever, and Dario Amodei. Language Models are Few-Shot Learners, 2020. URL <https://arxiv.org/abs/2005.14165>.
- Mark Chen, Jerry Tworek, Heewoo Jun, Qiming Yuan, Henrique Ponde de Oliveira Pinto, Jared Kaplan, et al. Evaluating Large Language Models Trained on Code, 2021. URL <https://arxiv.org/abs/2107.03374>.

- Zhe Chen, Weiyun Wang, Yue Cao, Yangzhou Liu, Zhangwei Gao, Erfei Cui, Jinguo Zhu, Shenglong Ye, Hao Tian, Zhaoyang Liu, et al. Expanding Performance Boundaries of Open-Source Multimodal Models with Model, Data, and Test-Time Scaling. *arXiv preprint arXiv:2412.05271*, 2024.
- Peter Clark, Isaac Cowhey, Oren Etzioni, Tushar Khot, Ashish Sabharwal, Carissa Schoenick, and Oyvind Tafjord. Think you have Solved Question Answering? Try ARC, the AI2 Reasoning Challenge. *ArXiv*, abs/1803.05457, 2018.
- Karl Cobbe, Vineet Kosaraju, Mohammad Bavarian, Mark Chen, Heewoo Jun, Lukasz Kaiser, Matthias Plappert, Jerry Tworek, Jacob Hilton, Reiichiro Nakano, Christopher Hesse, and John Schulman. Training Verifiers to Solve Math Word Problems, 2021. URL <https://arxiv.org/abs/2110.14168>.
- Wenliang Dai, Nayeon Lee, Boxin Wang, Zhuolin Yang, Zihan Liu, Jon Barker, Tuomas Rintamaki, Mohammad Shoeybi, Bryan Catanzaro, and Wei Ping. NVLM: Open Frontier-class Multimodal LLMs. *arXiv preprint arXiv:2409.11402*, 2024.
- Tri Dao and Albert Gu. Transformers are SSMS: Generalized Models and Efficient Algorithms Through Structured State Space Duality, 2024. URL <https://arxiv.org/abs/2405.21060>.
- Gemma Team @ Google DeepMind. Gemma 3 Technical Report, 2025. URL <https://arxiv.org/abs/2503.19786>.
- DeepSeek-AI. DeepSeek-R1: Incentivizing Reasoning Capability in LLMs via Reinforcement Learning, 2025a. URL <https://arxiv.org/abs/2501.12948>.
- DeepSeek-AI. DeepSeek-V3 Technical Report, 2025b. URL <https://arxiv.org/abs/2412.19437>.
- Haodong Duan, Junming Yang, Yuxuan Qiao, Xinyu Fang, Lin Chen, Yuan Liu, Xiaoyi Dong, Yuhang Zang, Pan Zhang, Jiaqi Wang, et al. VLMEvalKit: An Open-Source Toolkit for Evaluating Large Multi-Modality Models. In *Proceedings of the 32nd ACM International Conference on Multimedia*, pp. 11198–11201, 2024.
- Steven Feng, Shrimai Prabhumoye, Kezhi Kong, Dan Su, Mostofa Patwary, Mohammad Shoeybi, and Bryan Catanzaro. Maximize Your Data’s Potential: Enhancing LLM Accuracy with Two-Phase Pretraining, 2024. URL <https://arxiv.org/abs/2412.15285>.
- Shaona Ghosh, Prasoon Varshney, Makesh Narsimhan Sreedhar, Aishwarya Padmakumar, Traian Rebedea, Jibin Rajan Varghese, and Christopher Parisien. AEGIS2. 0: A Diverse AI Safety Dataset and Risks Taxonomy for Alignment of LLM Guardrails. *arXiv preprint arXiv:2501.09004*, 2025.
- Yash Goyal, Tejas Khot, Douglas Summers-Stay, Dhruv Batra, and Devi Parikh. Making the V in VQA Matter: Elevating the Role of Image Understanding in Visual Question Answering. In *Proceedings of the IEEE Conference on Computer Vision and Pattern Recognition*, pp. 6904–6913, 2017.
- Albert Gu and Tri Dao. Mamba: Linear-Time Sequence Modeling with Selective State Spaces, 2024. URL <https://arxiv.org/abs/2312.00752>.
- Dan Hendrycks, Collin Burns, Steven Basart, Andy Zou, Mantas Mazeika, Dawn Song, and Jacob Steinhardt. Measuring Massive Multitask Language Understanding, 2021a. URL <https://arxiv.org/abs/2009.03300>.

- Dan Hendrycks, Collin Burns, Saurav Kadavath, Akul Arora, Steven Basart, Eric Tang, Dawn Song, and Jacob Steinhardt. Measuring Mathematical Problem Solving With the MATH Dataset, 2021b. URL <https://arxiv.org/abs/2103.03874>.
- Geoffrey Hinton, Oriol Vinyals, and Jeff Dean. Distilling the Knowledge in a Neural Network, 2015.
- Cheng-Ping Hsieh, Simeng Sun, Samuel Kriman, Shantanu Acharya, Dima Rekish, Fei Jia, Yang Zhang, and Boris Ginsburg. RULER: What’s the Real Context Size of Your Long-Context Language Models?, 2024. URL <https://arxiv.org/abs/2404.06654>.
- Drew A Hudson and Christopher D Manning. GQA: A New Dataset for Real-World Visual Reasoning and Compositional Question Answering. In *Proceedings of the IEEE/CVF conference on computer vision and pattern recognition*, pp. 6700–6709, 2019.
- Kushal Kafle, Brian Price, Scott Cohen, and Christopher Kanan. DVQA: Understanding Data Visualizations via Question Answering. In *Proceedings of the IEEE Conference on Computer Vision and Pattern Recognition*, pp. 5648–5656, 2018.
- Ilia Karmanov, Amala Sanjay Deshmukh, Lukas Voegtle, Philipp Fischer, Kateryna Chumachenko, Timo Roman, Jarno Seppänen, Jupinder Parmar, Joseph Jennings, Andrew Tao, and Karan Sapra. Éclair – Extracting Content and Layout with Integrated Reading Order for Documents, 2025. URL <https://arxiv.org/abs/2502.04223>.
- Angelos Katharopoulos, Apoorv Vyas, Nikolaos Pappas, and François Fleuret. Transformers are RNNs: Fast Autoregressive Transformers with Linear Attention, 2020. URL <https://arxiv.org/abs/2006.16236>.
- Aniruddha Kembhavi, Mike Salvato, Eric Kolve, Minjoon Seo, Hannaneh Hajishirzi, and Ali Farhadi. A Diagram Is Worth A Dozen Images. In *ECCV*, 2016.
- Vijay Korthikanti, Jared Casper, Sangkug Lym, Lawrence McAfee, Michael Andersch, Mohammad Shoeybi, and Bryan Catanzaro. Reducing Activation Recomputation in Large Transformer Models, 2022. URL <https://arxiv.org/abs/2205.05198>.
- Ranjay Krishna, Yuke Zhu, Oliver Groth, Justin Johnson, Kenji Hata, Joshua Kravitz, Stephanie Chen, Yannis Kalantidis, Li-Jia Li, David A Shamma, et al. Visual Genome: Connecting Language and Vision Using Crowdsourced Dense Image Annotations. *International Journal of Computer Vision*, 123:32–73, 2017.
- Woosuk Kwon, Zhuohan Li, Siyuan Zhuang, Ying Sheng, Lianmin Zheng, Cody Hao Yu, Joseph E. Gonzalez, Hao Zhang, and Ion Stoica. Efficient Memory Management for Large Language Model Serving with PagedAttention, 2023. URL <https://arxiv.org/abs/2309.06180>.
- Jeffrey Li, Alex Fang, Georgios Smyrnis, Maor Ivgi, Matt Jordan, Samir Yitzhak Gadre, Hritik Bansal, Etash Guha, Sedrick Scott Keh, Kushal Arora, et al. DataComp-LM: In Search of the Next Generation of Training Sets for Language Models. *Advances in Neural Information Processing Systems*, 37:14200–14282, 2024.
- Junnan Li, Dongxu Li, Caiming Xiong, and Steven Hoi. BLIP: Bootstrapping Language-Image Pre-training for Unified Vision-Language Understanding and Generation. In *International Conference on Machine Learning*, pp. 12888–12900. PMLR, 2022.
- Zhiqi Li, Guo Chen, Shilong Liu, Shihao Wang, Vibashan VS, Yishen Ji, Shiyi Lan, Hao Zhang, Yilin Zhao, Subhashree Radhakrishnan, et al. Eagle 2: Building Post-Training Data Strategies from Scratch for Frontier Vision-Language Models. *arXiv preprint arXiv:2501.14818*, 2025.

- Opher Lieber, Barak Lenz, Hofit Bata, Gal Cohen, Jhonathan Osin, Itay Dalmedigos, Erez Safahi, Shaked Meiron, Yonatan Belinkov, Shai Shalev-Shwartz, Omri Abend, Raz Alon, Tomer Asida, Amir Bergman, Roman Glozman, Michael Gokhman, Avashalom Manevich, Nir Ratner, Noam Rozen, Erez Shwartz, Mor Zusman, and Yoav Shoham. Jamba: A Hybrid Transformer-Mamba Language Model, 2024. URL <https://arxiv.org/abs/2403.19887>.
- Tsung-Yi Lin, Michael Maire, Serge Belongie, Lubomir Bourdev, Ross Girshick, James Hays, Pietro Perona, Deva Ramanan, C. Lawrence Zitnick, and Piotr Dollár. Microsoft COCO: Common Objects in Context, 2015. URL <https://arxiv.org/abs/1405.0312>.
- Adam Dahlgren Lindström and Savitha Sam Abraham. CLEVR-Math: A Dataset for Compositional Language, Visual and Mathematical Reasoning. *arXiv preprint arXiv:2208.05358*, 2022.
- Haotian Liu, Chunyuan Li, Qingyang Wu, and Yong Jae Lee. Visual Instruction Tuning. *Advances in Neural Information Processing Systems*, 36:34892–34916, 2023a.
- Jiawei Liu, Chunqiu Steven Xia, Yuyao Wang, and Lingming Zhang. Is Your Code Generated by ChatGPT Really Correct? Rigorous Evaluation of Large Language Models for Code Generation. *arXiv preprint arXiv:2305.01210*, 2023b. doi: <https://doi.org/10.48550/arXiv.2305.01210>. URL <https://arxiv.org/abs/2305.01210>.
- Yuliang Liu, Zhang Li, Mingxin Huang, Biao Yang, Wenwen Yu, Chunyuan Li, Xucheng Yin, Chenglin Liu, Lianwen Jin, and Xiang Bai. OCRBench: On the Hidden Mystery of OCR in Large Multimodal Models, 2024. URL <https://arxiv.org/abs/2305.07895>.
- Pan Lu, Swaroop Mishra, Tanglin Xia, Liang Qiu, Kai-Wei Chang, Song-Chun Zhu, Oyvind Tafjord, Peter Clark, and Ashwin Kalyan. Learn to Explain: Multimodal Reasoning via Thought Chains for Science Question Answering. *Advances in Neural Information Processing Systems*, 35:2507–2521, 2022.
- Pan Lu, Hritik Bansal, Tony Xia, Jiacheng Liu, Chunyuan Li, Hannaneh Hajishirzi, Hao Cheng, Kai-Wei Chang, Michel Galley, and Jianfeng Gao. MathVista: Evaluating Mathematical Reasoning of Foundation Models in Visual Contexts. In *International Conference on Learning Representations (ICLR)*, 2024.
- Pratyush Maini, Skyler Seto, He Bai, David Grangier, Yizhe Zhang, and Navdeep Jaitly. Rephrasing the Web: A Recipe for Compute and Data-Efficient Language Modeling. In *ICLR 2024 Workshop on Navigating and Addressing Data Problems for Foundation Models*, 2024.
- Somshubra Majumdar, Vahid Noroozi, Sean Narenthiran, Aleksander Ficek, Jagadeesh Balam, and Boris Ginsburg. Genetic Instruct: Scaling up Synthetic Generation of Coding Instructions for Large Language Models. 2024. URL <https://arxiv.org/abs/2407.21077>.
- Andres Marafioti and Hugo Laurencon. Docmatix - A Huge Dataset for Document Visual Question Answering, 2024.
- Kenneth Marino, Mohammad Rastegari, Ali Farhadi, and Roozbeh Mottaghi. OK-VQA: A Visual Question Answering Benchmark Requiring External Knowledge. In *Proceedings of the IEEE/cvf conference on computer vision and pattern recognition*, pp. 3195–3204, 2019.
- Ahmed Masry, Do Xuan Long, Jia Qing Tan, Shafiq Joty, and Enamul Hoque. ChartQA: A Benchmark for Question Answering about Charts with Visual and Logical Reasoning. *arXiv preprint arXiv:2203.10244*, 2022.

- Minesh Mathew, Dimosthenis Karatzas, and CV Jawahar. DocVQA: A Dataset for VQA on Document Images. In *Proceedings of the IEEE/CVF Winter Conference on Applications of Computer Vision*, pp. 2200–2209, 2021.
- Llama Team @ Meta. The Llama 3 Herd of Models, 2024. URL <https://arxiv.org/abs/2407.21783>.
- Paulius Micikevicius, Dusan Stosic, Neil Burgess, Marius Cornea, Pradeep Dubey, Richard Grisenthwaite, Sangwon Ha, Alexander Heinecke, Patrick Judd, John Kamalu, Naveen Mellempudi, Stuart Oberman, Mohammad Shoeybi, Michael Siu, and Hao Wu. FP8 Formats for Deep Learning, 2022. URL <https://arxiv.org/abs/2209.05433>.
- Todor Mihaylov, Peter Clark, Tushar Khot, and Ashish Sabharwal. Can a Suit of Armor Conduct Electricity? A New Dataset for Open Book Question Answering, 2018. URL <https://arxiv.org/abs/1809.02789>.
- Anand Mishra, Shashank Shekhar, Ajeet Kumar Singh, and Anirban Chakraborty. OCR-VQA: Visual Question Answering by Reading Text in Images. In *2019 International Conference on Document Analysis and Recognition (ICDAR)*, pp. 947–952. IEEE, 2019.
- Niklas Muennighoff, Alexander Rush, Boaz Barak, Teven Le Scao, Nouamane Tazi, Aleksandra Piktus, Sampo Pyysalo, Thomas Wolf, and Colin A Raffel. Scaling Data-Constrained Language Models. *Advances in Neural Information Processing Systems*, 36, 2024.
- Saurav Muralidharan, Sharath Turuvekere Sreenivas, Raviraj Joshi, Marcin Chochowski, Mostofa Patwary, Mohammad Shoeybi, Bryan Catanzaro, Jan Kautz, and Pavlo Molchanov. Compact Language Models via Pruning and Knowledge Distillation, 2024. URL <https://arxiv.org/abs/2407.14679>.
- NVIDIA. Nemotron-4 340B Technical Report, 2024. URL <https://arxiv.org/abs/2406.11704>.
- NVIDIA. Floating-Point Computing and CUDA, 2025. URL <https://docs.nvidia.com/cuda/floating-point/index.html>.
- NVIDIA, Alisson Azzolini, Hannah Brandon, Prithvijit Chattopadhyay, Huayu Chen, Jinju Chu, Yin Cui, Jenna Diamond, Yifan Ding, Francesco Ferroni, Rama Govindaraju, Jinwei Gu, Siddharth Gururani, Imad El Hanafi, Zekun Hao, Jacob Huffman, Jingyi Jin, Brendan Johnson, Rizwan Khan, George Kurian, Elena Lantz, Nayeon Lee, Zhaoshuo Li, Xuan Li, Tsung-Yi Lin, Yen-Chen Lin, Ming-Yu Liu, Andrew Mathau, Yun Ni, Lindsey Pavao, Wei Ping, David W. Romero, Misha Smelyanskiy, Shuran Song, Lyne Tchammi, Andrew Z. Wang, Boxin Wang, Haoxiang Wang, Fangyin Wei, Jiashu Xu, Yao Xu, Xiaodong Yang, Zhuolin Yang, Xiaohui Zeng, and Zhe Zhang. Cosmos-Reason1: From Physical Common Sense To Embodied Reasoning, 2025. URL <https://arxiv.org/abs/2503.15558>.
- OpenAI. Learning to Reason with LLMs, 2025. URL <https://openai.com/index/learning-to-reason-with-llms/>.
- Vicente Ordonez, Girish Kulkarni, and Tamara Berg. Im2text: Describing Images using 1 Million Captioned Photographs. *Advances in Neural Information Processing Systems*, 24, 2011.
- Jupinder Parmar, Shrimai Prabhumoye, Joseph Jennings, Mostofa Patwary, Sandeep Subramanian, Dan Su, Chen Zhu, Deepak Narayanan, Aastha Jhunjhunwala, Ayush Dattagupta, Vibhu Jawa, Jiwei Liu, Ameya Mahabaleshwarkar, Osvald Nitski, Annika Brundyn, James Maki, Miguel Martinez, Jiaxuan You, John Kamalu, Patrick LeGresley, Denys Fridman, Jared Casper, Ashwath

- Aithal, Oleksii Kuchaiev, Mohammad Shoeybi, Jonathan Cohen, and Bryan Catanzaro. Nemotron-4 15B Technical Report. *arXiv preprint arXiv:2402.16819*, 2024. URL <https://arxiv.org/abs/2402.16819>.
- Keiran Paster, Marco Dos Santos, Zhangir Azerbayev, and Jimmy Ba. OpenWebMath: An Open Dataset of High-Quality Mathematical Web Text, 2023.
- Guilherme Penedo, Hynek Kydlíček, Anton Lozhkov, Margaret Mitchell, Colin A Raffel, Leandro Von Werra, Thomas Wolf, et al. The FineWeb datasets: Decanting the Web for the Finest Text Data at Scale. *Advances in Neural Information Processing Systems*, 37:30811–30849, 2024.
- Qwen. Qwen2.5 Technical Report, 2025. URL <https://arxiv.org/abs/2412.15115>.
- Samy Rajbhandari, Jeff Rasley, Olatunji Ruwase, and Yuxiong He. ZeRO: Memory Optimizations Toward Training Trillion Parameter Models, 2020. URL <https://arxiv.org/abs/1910.02054>.
- Keisuke Sakaguchi, Ronan Le Bras, Chandra Bhagavatula, and Yejin Choi. WinoGrande: An Adversarial Winograd Schema Challenge at Scale, 2019. URL <https://arxiv.org/abs/1907.10641>.
- Piyush Sharma, Nan Ding, Sebastian Goodman, and Radu Soricut. Conceptual Captions: A Cleaned, Hypernamed, Image Alt-text Dataset for Automatic Image Captioning. In *Proceedings of the 56th Annual Meeting of the Association for Computational Linguistics (Volume 1: Long Papers)*, pp. 2556–2565, 2018.
- Mohammad Shoeybi, Mostofa Patwary, Raul Puri, Patrick LeGresley, Jared Casper, and Bryan Catanzaro. Megatron-LM: Training Multi-Billion Parameter Language Models Using Model Parallelism, 2020. URL <https://arxiv.org/abs/1909.08053>.
- Amanpreet Singh, Vivek Natarajan, Meet Shah, Yu Jiang, Xinlei Chen, Dhruv Batra, Devi Parikh, and Marcus Rohrbach. Towards VQA Models That Can Read. In *Proceedings of the IEEE/CVF conference on computer vision and pattern recognition*, pp. 8317–8326, 2019.
- David R. So, Wojciech Mańke, Hanxiao Liu, Zihang Dai, Noam Shazeer, and Quoc V. Le. Primer: Searching for Efficient Transformers for Language Modeling, 2022. URL <https://arxiv.org/abs/2109.08668>.
- Sharath Turuvekere Sreenivas, Saurav Muralidharan, Raviraj Joshi, Marcin Chochowski, Ameya Sunil Mahabaleshwarkar, Gerald Shen, Jiaqi Zeng, Zijia Chen, Yoshi Suhara, Shizhe Diao, Chenhan Yu, Wei-Chun Chen, Hayley Ross, Oluwatobi Olabiyi, Ashwath Aithal, Oleksii Kuchaiev, Daniel Korzekwa, Pavlo Molchanov, Mostofa Patwary, Mohammad Shoeybi, Jan Kautz, and Bryan Catanzaro. LLM Pruning and Distillation in Practice: The Minitron Approach, 2024. URL <https://arxiv.org/abs/2408.11796>.
- Dan Su, Kezhi Kong, Ying Lin, Joseph Jennings, Brandon Norick, Markus Kliegl, Mostofa Patwary, Mohammad Shoeybi, and Bryan Catanzaro. Nemotron-CC: Transforming Common Crawl into a Refined Long-Horizon Pretraining Dataset, 2024. URL <https://arxiv.org/abs/2412.02595>.
- Jianlin Su, Yu Lu, Shengfeng Pan, Ahmed Murtadha, Bo Wen, and Yunfeng Liu. RoFormer: Enhanced Transformer with Rotary Position Embedding, 2023. URL <https://arxiv.org/abs/2104.09864>.
- Shengyang Sun, Yian Zhang, Alexander Bukharin, David Mosallanezhad, Jiaqi Zeng, Soumye Singhal, Gerald Shen, Adithya Renduchintala, Tugrul Konuk, Yi Dong, Zhilin Wang, Dmitry Chichkov, Olivier Delalleau, and Oleksii Kuchaiev. Reward-aware Preference Optimization: A

- Unified Mathematical Framework for Model Alignment, 2025. URL <https://arxiv.org/abs/2502.00203>.
- Shubham Toshniwal, Wei Du, Ivan Moshkov, Branislav Kisacanic, Alexan Ayrapetyan, and Igor Gitman. OpenMathInstruct-2: Accelerating AI for Math with Massive Open-Source Instruction Data. *arXiv preprint arXiv:2410.01560*, 2024.
- Ashish Vaswani, Noam Shazeer, Niki Parmar, Jakob Uszkoreit, Llion Jones, Aidan N. Gomez, Lukasz Kaiser, and Illia Polosukhin. Attention Is All You Need, 2023. URL <https://arxiv.org/abs/1706.03762>.
- Andreas Veit, Tomas Matera, Lukas Neumann, Jiri Matas, and Serge Belongie. COCO-Text: Dataset and Benchmark for Text Detection and Recognition in Natural Images. 2016. URL <https://arxiv.org/abs/1601.07140>.
- Roger Waleffe, Wonmin Byeon, Duncan Riach, Brandon Norick, Vijay Korthikanti, Tri Dao, Albert Gu, Ali Hatamizadeh, Sudhakar Singh, Deepak Narayanan, Garvit Kulshreshtha, Vartika Singh, Jared Casper, Jan Kautz, Mohammad Shoeybi, and Bryan Catanzaro. An Empirical Study of Mamba-based Language Models, 2024. URL <https://arxiv.org/abs/2406.07887>.
- Yubo Wang, Xueguang Ma, Ge Zhang, Yuansheng Ni, Abhranil Chandra, Shiguang Guo, Weiming Ren, Aaran Arulraj, Xuan He, Ziyang Jiang, Tianle Li, Max Ku, Kai Wang, Alex Zhuang, Rongqi Fan, Xiang Yue, and Wenhui Chen. MMLU-Pro: A More Robust and Challenging Multi-Task Language Understanding Benchmark, 2024. URL <https://arxiv.org/abs/2406.01574>.
- xAI. Grok-1.5 Vision Preview: Connecting the Digital and Physical Worlds with our First Multimodal Model, 2024.
- Xiang Yue, Yuansheng Ni, Kai Zhang, Tianyu Zheng, Ruoqi Liu, Ge Zhang, Samuel Stevens, Dongfu Jiang, Weiming Ren, Yuxuan Sun, Cong Wei, Botao Yu, Ruibin Yuan, Renliang Sun, Ming Yin, Boyuan Zheng, Zhenzhu Yang, Yibo Liu, Wenhao Huang, Huan Sun, Yu Su, and Wenhui Chen. MMMU: A Massive Multi-discipline Multimodal Understanding and Reasoning Benchmark for Expert AGI. In *Proceedings of CVPR*, 2024.
- Rowan Zellers, Ari Holtzman, Yonatan Bisk, Ali Farhadi, and Yejin Choi. HellaSwag: Can a Machine Really Finish Your Sentence?, 2019. URL <https://arxiv.org/abs/1905.07830>.
- Biao Zhang and Rico Sennrich. Root Mean Square Layer Normalization, 2019. URL <https://arxiv.org/abs/1910.07467>.
- Jeffrey Zhou, Tianjian Lu, Swaroop Mishra, Siddhartha Brahma, Sujoy Basu, Yi Luan, Denny Zhou, and Le Hou. Instruction-following Evaluation for Large Language Models. *arXiv preprint arXiv:2311.07911*, 2023.